water

IMPACT FACTOR 3.4

CITESCORE 5.5

Article

Assessment of the Impact of Anthropogenic Evolution and Natural Processes on Shoreline Dynamics Using Multi-Temporal Satellite Images and Statistical Analysis

Perumal Balakrishnan, Ammar Abulibdeh and Tahsin Abul Kasem Kabir

Special Issue

Coastal Processes and Climate Change

Edited by

Prof. Dr. Mohamed Hereher and Prof. Dr. Ayad M. Fadhil Al-Quraishi

MDPI

https://doi.org/10.3390/w15081440

water

MDPI

Article

Assessment of the Impact of Anthropogenic Evolution and Natural Processes on Shoreline Dynamics Using Multi-Temporal Satellite Images and Statistical Analysis

Perumal Balakrishnan [1], Ammar Abulibdeh [2,*] and Tahsin Abul Kasem Kabir [1]

[1] Department of Biological & Environmental Sciences, Qatar University, Doha P.O. Box 2713, Qatar; bala@qu.edu.qa (P.B.)
[2] Applied Geography and GIS Program, Department of Humanities, College of Arts and Sciences, Qatar University, Doha P.O. Box 2713, Qatar
* Correspondence: aabulibdeh@qu.edu.qa

Abstract: This research aims to examine changes in the eastern part of Qatar's shoreline from 1982 to 2018 by means of satellite imagery. Five different time periods, namely 1982, 1992, 2002, 2013, and 2018, were analysed to determine shoreline movements and shoreline variations. Techniques such as maximum likelihood classification, the normalised difference vegetation index, and tasselled cap transformation were utilised to extract the shoreline data. Linear regression rate statistics were used to quantify the rate of shoreline variations. The results indicate that the majority of shoreline accretion is a result of human activities such as coastal construction, land reclamation, and building artificial islands, which are associated with the high economic activity over the past two decades. Significant changes were observed in Lusail City, The Pearl, and Hamad International Airport (HIA). Natural sediment accumulation was also observed in Al Wakra and on the southern side of HIA. In general, there were more land gains than losses throughout the study period, and the shoreline increased by twice its previous length. The field survey confirmed the presence of sandy and rocky beaches, as well as a shoreline with protective structures such as natural limestone rocks and concrete reinforcement.

Keywords: shoreline dynamics; multi-temporal satellite images; statistical analysis; anthropogenic activities; Qatar

Citation: Balakrishnan, P.; Abulibdeh, A.; Abul Kasem Kabir, T. Assessment of the Impact of Anthropogenic Evolution and Natural Processes on Shoreline Dynamics Using Multi-Temporal Satellite Images and Statistical Analysis. *Water* **2023**, *15*, 1440. https://doi.org/10.3390/w15081440

Academic Editors: Mohamed Hereher and Ayad M. Fadhil Al-Quraishi

Received: 1 February 2023
Revised: 23 March 2023
Accepted: 24 March 2023
Published: 7 April 2023

1. Introduction

The shoreline is a highly dynamic feature that changes continually due to interactions between oceans and land [1–3]. Measuring the rate of shoreline changes is crucial for effective coastal management and monitoring, especially for tracking coastal accretion and erosion [4]. The alteration of shorelines can have a significant impact on the socioeconomic and demographic characteristics of coastal areas [1,5,6], the degradation of coastal ecosystems [7–9], environmental consequences for aquatic ecosystems [10], and geomorphic responses [11–13].

Coastal ecosystems, which have multiple functions, are under increasing stress from both human activities and natural processes such as the growing population, coastal erosion, sea level rises, industrialisation, trade, over-exploitation of resources, tourism, and accelerated urbanisation [11,14–17]. These physical and human-induced changes have significant environmental consequences [4,18,19]. The natural changes are linked to geomorphic, hydrodynamic, climatic, tectonic, and hydrodynamic processes such as tides, erosion and deposition, coast protection structures, and currents, and can occur over both short and long periods [14,17,20–22]. Human impacts include erosion and deposition patterns, as well as increased loads of nutrients and toxic chemicals. Assessing the dynamic nature of coastal transition zones in terms of land, water, air, and human activities is challenging because of the rapid changes induced by both human activities and natural

processes. The dynamic characteristics of shorelines are shaped by development pressures, and require ongoing monitoring [23,24].

The study of shoreline changes is important for determining the impact of sea level rises, erosion, and accretion patterns, and for disaster and development planning [25]. Monitoring shorelines serves as a way in which to monitor and predict environmental changes in coastal zones over time [26]. Therefore, analysing shoreline change dynamics in terms of shape and position over time is an essential process for the management and monitoring of coastal areas, and can be significant in the future planning of the placement of urban landscapes and buildings [14].

Different approaches have been used to detect and monitor shoreline changes over space and time. For monitoring and managing shoreline changes, geospatial and remote sensing (RS) technologies have been utilised and proven to be extremely useful approaches [4]. Traditional field methods, geographic information systems (GIS), and RS techniques have become increasingly essential due to their ability to provide and analyse historical snapshots of shoreline displacements with higher accuracy [1,2,27]. Utilising satellite imagery and geospatial technology in coastal management and the monitoring of changes in shorelines is significant because of the high-accuracy mapping, reduction in manual errors, synoptic coverage, unbiased results of these approaches, and cost-effectiveness [3,28–30]. Satellite imagery is suitable for mapping and updating shoreline dynamics due to its capability of repetitive coverage, accuracy, and multispectral nature, as well as being a cost-effective tool [4,31,32]. Furthermore, the water–land interface is well defined by the digital imagery provided in infrared spectral bands from remote sensing satellites [33,34].

Several GIS and RS techniques have been used to monitor shoreline changes, such as the composition of modern light detection and ranging (LIDAR) [35–37], an airborne laser scanner [38], video technology [39], and synthetic aperture radar (SAR) imagery [40]. To reduce the cost of data acquisition, multispectral and aerial satellite imagery are used to efficiently compare multi-temporal images [31,41]. Aerial photos and multispectral satellite imagery have been used in previous studies to detect historical shoreline changes [42–45]. Duru [1] used six multi-temporal satellite images from Landsat to analyse historical shoreline changes between 1975 and 2016. The modified normalised difference water index (MNDWI), the normalised difference water index (NDWI), and supervised classification techniques were used in the analysis. Historical shoreline change rates were computed by using the Digital Shoreline Analysis System (DSAS). The average rate of shoreline change was 2.7 m/year for the entire coast with an uncertainty of 0.2 m/year. Elnabwy et al. [46] investigated accreted and eroded areas for 15 km of the coastal zone between 1985 and 2018 by means of Landsat satellite images. They classified and rectified the images using a supported vector machine (SVM). They found a dramatic erosion of 2.1 km^2 on the eastern side and a total accretion area of 14.90 km^2 of the southeastern side of the study area. Srinivasu et al. [47] revealed a reversal in the North Indian Ocean sea level decadal trend between 1993 and 2013 using ocean reanalysis, satellite, in situ data, and model simulations after removing the global mean sea level rise. They found that the sea level fell between 1993 and 2003 and, conversely, rose sharply between 2004 and 2013. Randazzo et al. [48] studied the shoreline dynamics on the coast of San Vito Lo Capo and proposed a new framework for the processing of GeoEye-1 satellite images. They found that using such new techniques will overcome the limitations in traditional methods. Zollini et al. [49] used a new algorithm, J-Net Dynamic, and found that this experimental algorithm is more effective than other algorithms used for detecting shoreline dynamic changes.

The aim of this study is to examine shoreline morphological change (erosion and accretion) rates along the east coast of Qatar by means of multi-temporal satellite imagery, classification techniques, and statistical methods. The study aims to detect and identify shoreline changes in the Doha coast since 1982 and study changes in the length and shape of the coastline during this period. This is the first research of its kind in the country, and it aims to provide new information and understanding regarding shoreline change trends

resulting from human activities and practices. The findings will aid in the management of current and future development projects to ensure responsible coastal management.

2. Materials and Methods

2.1. Profile of the Study Area

The state of Qatar is located in the Middle East region to the east of the Arabian Peninsula at 25°30′ N and 51°15′ E, bordering the Arabian Gulf and Saudi Arabia, with a geographical area of 11,437 km^2 (as shown in Figure 1). Following its establishment in 1971, the country witnessed rapid economic and population growth driven by the discovery of large oil and gas reserves [50–53]. The population of the country increased exponentially from 0.46 million in 1960 to 2.8 million in 2019 due to the influx of the expatriate population driven by the need of workers to satisfy economic development and, recently, organise the 2022 FIFA World Cup [54–58]. Furthermore, the country adopted an ambitious 2030 development vision for human, economic, environmental, and social development, which has led to large-scale investment projects, massive urban development, a significant growth rate in real gross domestic product (GDP), and rising governmental expenditure [59–63].

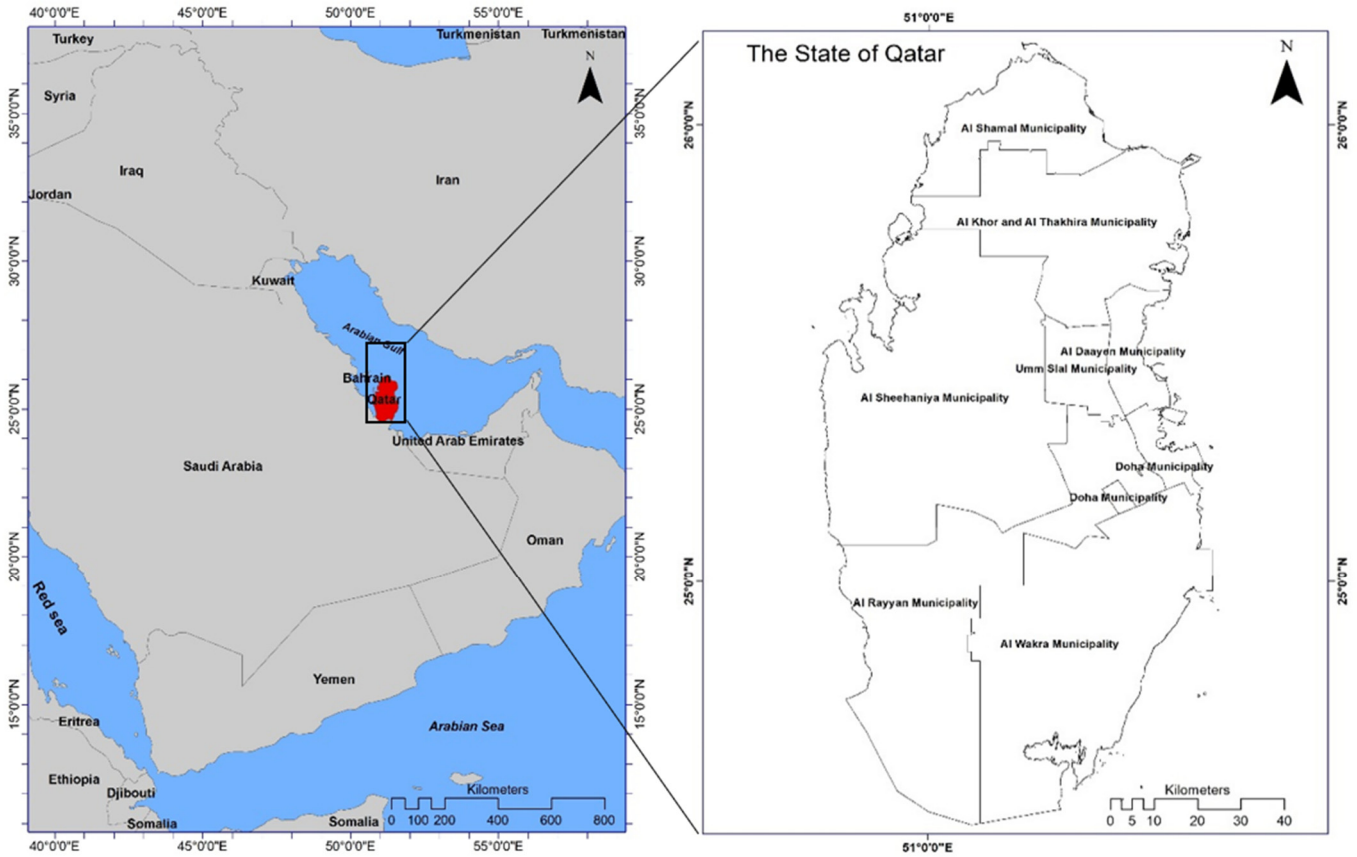

Figure 1. Map showing the location of Qatar [54].

The estimated length of Qatar's shoreline is 560 km and, due to the harsh climatic and geographical conditions, residents have always settled around the country's shoreline. Since the harsh desert of Qatar does not allow much agriculture, the shallow seawater around Qatar provides the necessary livestock for its people. Before oil and gas, the main sources of income and survival were marine fish and pearl diving. Since then, the population of Qatar has continued growing around the shoreline, especially in the eastern part. Therefore, most of the shoreline changes around major cities are due to human activities.

To understand the coastal area changes in Qatar's shoreline, the eastern region of the country, from Lusail to the Al Wakra shoreline, has been chosen for this research. The selected study area is from latitude 25°159′ N to 25°430′ N and from longitude 51°615′ E to 51°532′ E, connected to the western part of the Arabian Gulf (Figure 2). The shoreline of this area is characterised by the tide, which is high in winter and then decreases in spring, followed by summer, and in autumn, the tide has the lowest values [64] and the rainfall is low. Over the last few decades, there has been high human activity such as land reclamation and dredging in this area. All over the Persian/Arabian Gulf, the coastline has changed by more than 40%, and marine ecosystems are impacted heavily by land reclamation by means of dredging [65]. This land reclamation started as early as the 1970s in Qatar to expand the city centre with the growing urban needs. The reclamation continued to create the Pearl Project, which is new land spanning 400 ha. Lusail City, an expanse of 35 km^2, is a further huge area of land reclaimed from the sea in northern Doha. Hamad International Airport in the south of Doha is approximately 22 km^2, and 60% of this is reclaimed land [66]. Major projects such as Hamad Sea Port [67], the new Doha International Airport [68], the Sharq Crossing [69], and some artificial islands are all developed along the coast, dredging up the sea.

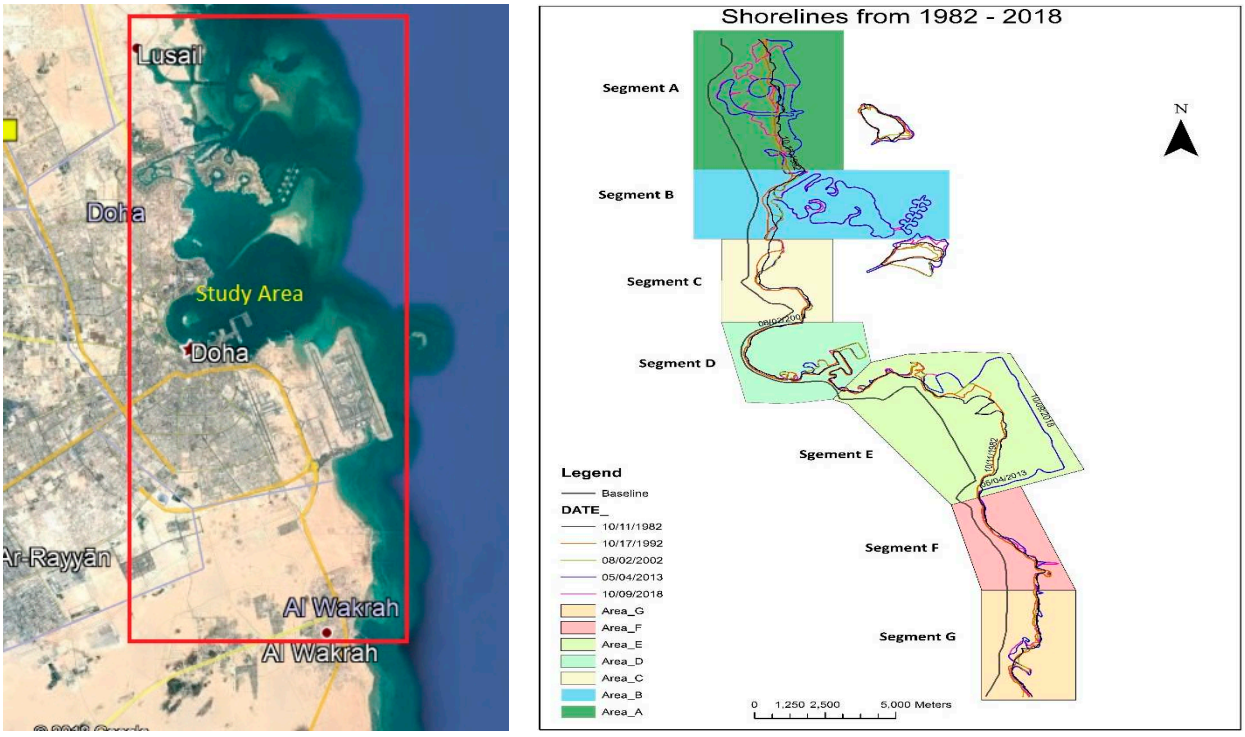

(**a**) (**b**)

Figure 2. (**a**) Study area, (**b**) study area segments.

The shoreline of the study area belongs to three major cities, namely Lusail, Doha, and Al Wakra (see Figure 2). Furthermore, the study area contains 14 zones (as shown in Table 1). The table shows the names and areas of the zones sequentially from north to south of the study area. Since the study area is too large to analyse in one frame, the area is divided into seven segments based on zones defined by the Ministry of Municipality of Qatar. The segmented area allows us to see the shoreline changes more visually and also makes the data easy to interpret. Figure 3 shows a map with all seven segments and five shorelines from 1982 to 2019.

Table 1. Zone number and its allocated areas.

Zone Number	Name of the Areas	Study Segments
69	Lusail	A
66	The Pearl, Leqtaifiya, Al Qassar	B
61	Al Qassar, Al Dafna	C
60	Al Dafna	D
12	Rumaila, Al Bidda	
2	Al Bidda	
1	Al Jasra	
7	Al Souq	
19	Doha Port	
18	Slata, Al Mirqab	
28	Al Khulaifat, Ras Bu Abboud	E
29	Ras Bu Abboud	
49	Hamad International Airport	
49	Hamad International Airport	F
90	Al Wakra	G

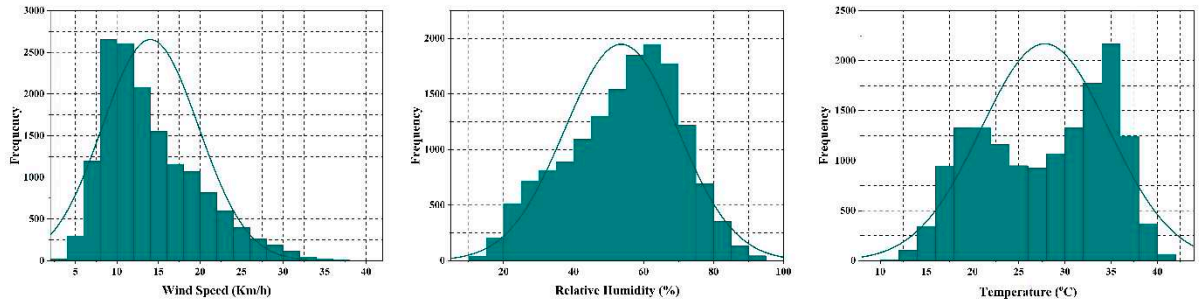

(**a**)

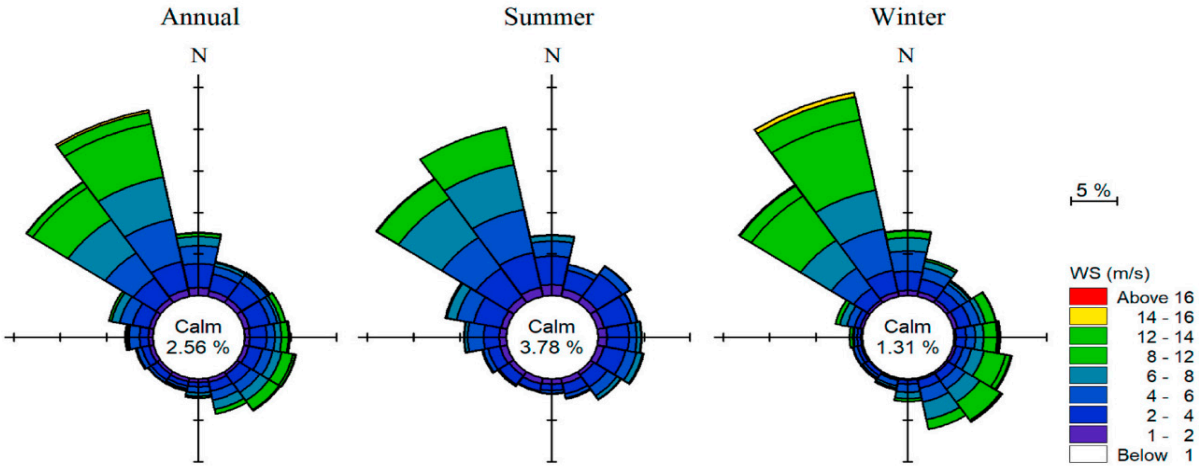

(**b**)

Figure 3. (**a**) Annual wind speed, relative humidity, and temperature in Qatar, (**b**) annual wind speed off Fuwairit in 2019 [68].

Marine Climate Analysis

Surface waves and winds are important factors that have a significant influence on the dynamics of the shoreline. They influence the movement of sediment and the longshore current. Therefore, it is essential to consider the effects of surface waves and winds when designing offshore and coastal structures and determining how to load and unload materials as well as to exploit traditional resources [68]. The Arabian Gulf is located in a tropical and subtropical desert climate (BWh) and is a semi-enclosed sea. The climate of the Arabian Gulf area is characterised by a hot summer and a moderate winter, northerly winds, high evaporation, dust storms, and very low precipitation. The summer season extends between April and October, and the average annual temperature ranges between 32 and 38 °C (as shown in Figure 3a). Moreover, the precipitation and the relative humidity are very low during the summer season and increase in the winter season, which extends between November and March. The average temperature in the winter season ranges between 13 and 23 °C [51].

Throughout the year, the state of Qatar is influenced by winds from different directions. The prevailing winds are from the north and northwest, particularly in the summer season and on the northern coast of the country, where the northerly (Shamal) winds are dominant (Figure 3b). In the winter, the easterly and south–southeasterly winds are more dominant [68–70]. The waves in the Arabian Gulf follow the prevailing wind patterns. However, the orientation and deflection of the Strait of Hormuz, which is located to the south of the Arabian Gulf, disable the long-period swells from the Sea of Oman on the other side of the Strait. Nevertheless, complex wave conditions near the Gulf entrance are sometimes created due to the interaction between wind seas/young swells generated on either side of the Strait as well as the complex bottom topography [68,71–73]. This phenomenon has a minor impact on the wave climate near the shoreline of Qatar.

2.2. Data Source

Landsat images are used as the primary source of satellite data. Since our focus is on analysing and comparing shoreline changes over the last 36 years, to monitor changes in the shoreline of the Doha coast due to anthropogenic activities, five images are obtained from satellite sensors, which include the USGS Earth Explorer web service scenes of the Landsat-3 Multispectral Scanner (MSS), Landsat-5 Thematic Mapper (TM), and Landsat-8 Operational Land Imager and Thermal Infrared Sensor (OLI-TRIS), between the years 1982 and 2018 (Table 2). Using the satellite data, changes in the coastline can be monitored over the short term as well as the long term. Minute changes in the shoreline, however, remain undetected due to the spatial resolution of 30 m and 60 m in the satellite images. To overcome this, a higher spatial resolution may be used. Thus, it is confirmed that the boundary detected between the shoreline and the sea via Landsat remains unaffected by the tidal motion. The 1982 data were obtained from Landsat 3 satellite images. The images were captured using a multispectral scanner (MSS) sensor (landsat.usgs.gov). A false colour composite (FCC) satellite image of the year 1982 is shown in Figure 4a. The 1992 data were obtained from Landsat 5 satellite images, which were captured using a thematic mapper (TM) sensor (landsat.usgs.gov). The TM sensor has seven bands, all of which take 30 × 30 m resolution images except for the thermal band, which has a 120 × 120 m resolution. A false colour composite satellite image of the year 1992 is shown in Figure 4b. The 2002 data were obtained from Landsat 7 satellite images, which were captured using an Enhanced Thematic Mapper Plus (ETM+) sensor. A false colour composite satellite image of the year 2002 is shown in Figure 4c. The most recent Landsat satellite data are for the years 2013 and 2018. False colour composite satellite images for 2013 and 2018 are shown in Figure 4d,e.

Table 2. List of satellite images used in this study, showing their properties.

Date of Acquisition	SPACECRAFT ID	SENSOR ID	Resolution in Meters	Size (Row/Path)
10/11/1982	Landsat_3	MSS	60	42/175
10/17/1992	Landsat_5	TM	30	43/162
8/2/2002	Landsat_5	TM	30	43/162
5/4/2013	Landsat_8	OLI	30	42/163
10/9/2018	Landsat_8	OLI-TRIS	30	42/163

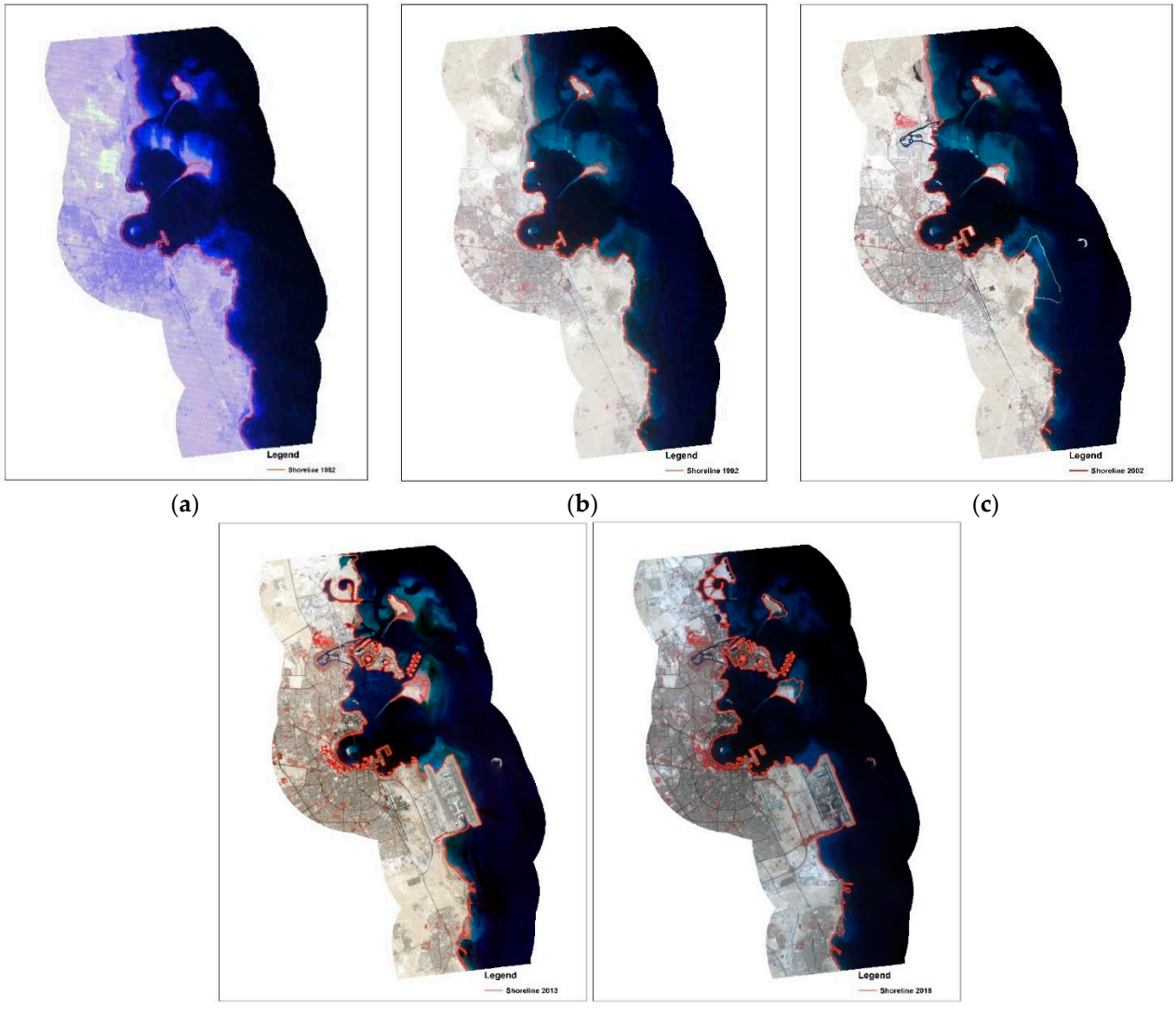

Figure 4. False colour composite image of (**a**) 1982, (**b**) 1992, (**c**) 2002, (**d**) 2013, and (**e**) 2018.

2.3. Methods

Figure 5 shows a flowchart of the various methodological approaches used in this study. Detailed explanations are provided in the subsequent sections.

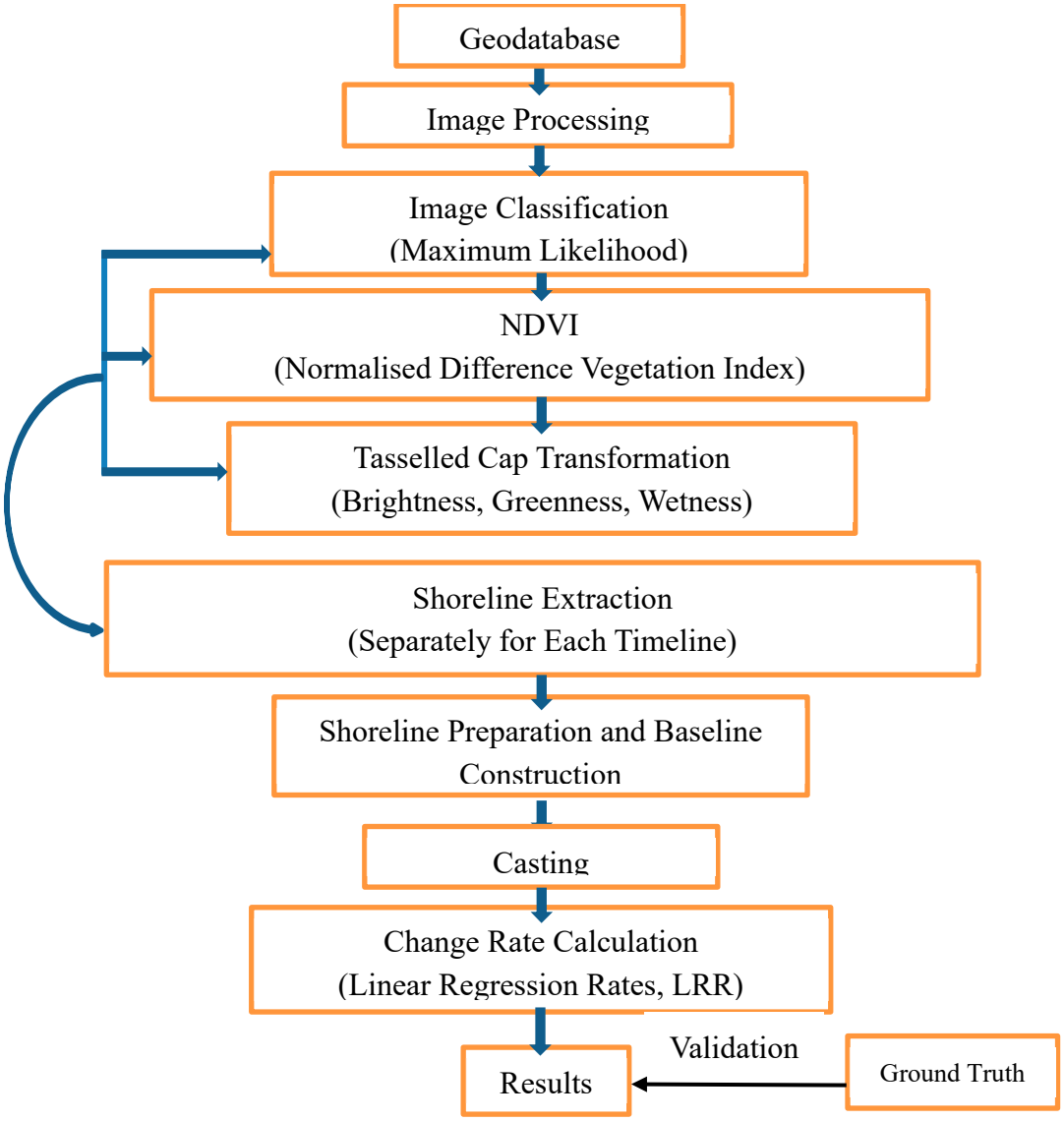

Figure 5. Flowchart of the methodology.

2.3.1. Geodatabase Development

This study employs Landsat imagery as a key data source for a spatiotemporal evaluation of the dynamics of shoreline changes. The collected imagery data are stored in a geodatabase, which serves as the source for the transect feature class generated by the program and analysed via the Digital Shoreline Analysis System (DSAS) software. The purpose of the geodatabase is to determine shoreline segment positions, assign attributes (ID, date, shape, length, uncertainty) to each segment, and compile the five shoreline positions into a single shapefile for a rate calculation.

2.3.2. Remote Sensing Image Processing

This process prepares satellite images for further analysis. Landsat MSS, TM, ETM, and OLI images are corrected for geometry by means of ground control points obtained by comparing remote sensing images with 1:5000 topographic maps. Stripping defects are avoided and the images are then clipped to the study area. Geometric and radiometric corrections are applied in order to reduce atmospheric effects, and cubic polynomial fitting is used for correction calculations. Bilinear interpolation is used to resample pixels, yielding a precision-corrected image for classification tests. The error is less than one pixel. Time linear stretch processing is performed to exclude intervals distributed across 256 greyscales,

and the images are improved for contrast and definition to simplify the interpretation of land categories. An RGB543 false colour composite is created from the bands with the most information and low redundancy [74,75].

2.3.3. Image Enhancement and Visual Interpretation

Image enhancement was applied in order to improve the clarity of features and the visual interpretability of the images [76]. Contrast stretching was performed, and false colour composites were produced. Screen digitising was used to interpret the FCC and identify easily recognisable land cover classes such as urban and sabkha. Visual interpretation was necessary in some cases to separate spectrally confused classes that could not be properly separated by supervised classification.

2.3.4. Vegetation Detection

The next step was to calculate the normalised difference vegetation index (NDVI), which measures the greenness of land surfaces and provides a standardised method for comparing vegetation greenness across satellite images [19]. NDVI values range from −1.0 (water) to 1.0 (dense green vegetation), with values near zero mainly representing rock and bare soil. The NDVI takes advantage of the contrast between chlorophyll pigment absorptions in the red band and the high reflectivity of plant materials in the near-infrared (NIR) band. The NDVI is calculated according to the following formula:

$$\text{NDVI} = \frac{IR - R}{IR + R} \tag{1}$$

where IR represents the pixel values from the infrared band and R represents the pixel values from the red band.

2.3.5. Water Detection

To detect and measure the extent of surface water, we used the normalised difference water index (NDWI). This index helps to identify surface water in vegetation and other surfaces by using satellite imagery green and near-infrared bands. The NDWI is calculated using the following equation:

$$\text{NDWI} = [(\text{Band 2} - \text{Band 4})/(\text{Band 2} + \text{Band 4})] \tag{2}$$

where Band 2 represents green light reflectance and Band 4 represents near-infrared (NIR) reflectance. Values of the NDWI that are greater than zero represent the water surface, and values less than or equal to zero represent non-water areas.

2.3.6. Tasselled Cap Transformation

The proponents of tasselled cap analysis are Kauth and Thomas, and it is now known as Kauth–Thomas transformation [77]. It was developed to analyse vegetation map and urban development changes by using numerous satellite sensor data. Tasselled cap transformation of principal component analysis transforms raster image data into a fresh coordinate system with a new set of orthogonal axes. Here, a three-component axis is created, namely brightness, greenness, and wetness. The six total bands of the Landsat series are used in a linear combination to estimate the (i) brightness, (ii) greenness, and (iii) wetness indices of the pixel [78,79]. The six bands used are visible and infrared bands, namely (i) blue (visible), (ii) green (visible), (iii) red (visible), (iv) near infrared (NIR), (v) shortwave infrared (SWIR-1), and (vi) mid-infrared (SWIR-2), respectively. For the tasselled cap analysis, Landsat 5 and 8 OLI imagery is used and three TCT indices are generated for the Doha coast.

Brightness is the total sum of all six reflective bands. This process is responsible for changing the total reflectance of those physical features that are only affected by this type of change. Therefore, feature characteristics such as particle size distribution of soil are

clearly observed in brightness [80]. On the other hand, an increase in vegetation density generally has a tendency to increase the NIR response and decrease the visible response. The second feature of tasselled cap transformation is greenness. This process involves contrasts between the total sum of visible and NIR bands [81,82]. In this process, a different test result shows that the reflectance of two long infrared bands causes them to cancel each other out. Therefore, the blue band mainly represents the spectral range of green vegetation. Wetness is the third feature of tasselled cap transformation. This feature provides entirely new information in comparison to the other two. This feature contrasts the total sum of all visible bands, NIR bands, and long infrared bands [83].

2.3.7. Shoreline Extraction

The shoreline position extracted in this study is not corrected pertaining to the tidal effect. The Qatar peninsula has a tidal amplitude of 1.6 m, and the smallest tidal amplitude is that of Salwa [84]. Usually, in waters bordering the shore (inshore) of Qatar, the wave height is around 30 cm, which can rise up to 1.52 m. Far from the shore (offshore), however, the waves can measure between 0.30 and 1.22 m. They can even rise to a height of 4.27 to 4.57 m during the Al Shamal winds [84]. The monitoring station located at Doha Port estimated that the sea level increased by 1.47 mm/year as per the sea level changes from 1976 to 2013. This was revised to an estimated 2.8 mm/year from 1993 to 2013. Shoreline extraction in remote sensing relies on the different spectral responses of water and land at various wavelengths [82]. Water absorbs most of the near- and mid-infrared radiation, resulting in low reflectance and allowing shoreline detection by means of a single-band infrared image. This can be carried out through histogram thresholding of Band 5 of TM or ETM+ imagery. However, this method is not entirely accurate, as the threshold value between water and land can vary and is difficult to determine from the histogram. An alternative technique is the band ratio method, which involves using two conditions (Band 2/Band 4 and Band 2/Band 5) to create binary image 1. Binary image 2 is created through histogram thresholding of Band 5, and binary image 3 is created by multiplying binary images 1 and 2.

2.3.8. Shoreline Preparation and Change Analysis

Shoreline areas undergoing accretion or erosion were measured using polygon–line intersections and polygon overlays. Each historical shoreline layer of the selected portion of the coast was coded as closed polylines. The methods used to measure accretion/erosion followed the following sequence: the first step was to draw a rectangular polygon (using new polylines) to enclose the study area. This served as a boundary polygon for all subsequent operations. The second step encompassed the intersection of each historical shoreline with the boundary polygon, dividing it into land and water polygons, coded topologically as polygons. The third step involved processing historical shorelines as land and water polygons, comparing two selected layers to produce a set of polygons with different characteristics, as well as identifying areas of erosion, accretion, or non-change through an analysis of the resulting polygon attribute table. This was accomplished by intersecting the two selected layers and using ArcMap spatial queries and functions to measure the changes in land.

2.3.9. Casting Transects

The topological constrained transect method (TCTM) uses dynamic segmentation to analyse a shoreline's displacement. It operates by using transects, which are polylines with a starting point, an endpoint at the most recent historical shoreline, and intermediate vertices at intermediate shorelines. The TCTM links equivalent critical points on historical shorelines by transects once the segments for analysis are chosen [83]. A proportional estimation of the corresponding points on different shorelines is performed from shoreline to shoreline, not using perpendicular lines. This guarantees the equal spacing of interpolated points and a consistent number of points over the corresponding segments. The resulting

transects consist of multiple links, each with its own length and direction, and the number of links per transect depends on the number of historical shorelines.

2.3.10. Geometric Correction

Accurate registration of multi-temporal remote sensing data at a pixel level is critical for change detection, as registration errors can be mistaken for land cover and land use changes, resulting in an overestimation of actual changes. In this analysis, each pixel is evaluated individually. Thus, any missed registration greater than one pixel will result in incorrect change detection. To avoid this, the root mean square error (RMSE) between two dates should not exceed 0.5 pixels. In this study, the images are geocoded using ground control points from 1980 topographic maps with a scale of 1:5000, and the 2019 image is corrected through geometric correction.

2.3.11. Uncertainty Quantification

In ArcGIS, the Dynamic Shoreline Analysis System (DSAS) calculates erosion and accretion rates along with extracted shorelines. Readers can refer to [85,86] for more information on DSAS. The feature class storing the shorelines also includes an attribute table with two fields: date and uncertainty. The latter is used only for weighted linear regression calculations and determined using the following equation:

$$Ut = \pm \sqrt{(Es^2 + Etd^2 + Ec^2 + Ed^2 + Ep^2 + Er^2 + Ets^2)} \quad (3)$$

where:

Es = seasonal error;
Etd = tidal fluctuation error;
Ec = conversion error;
Ed = digitising error;
Ep = pixel error;
Er = rectification error;
Ets = T-sheet plotting error.

For aerial imagery, the parameters Ec and Ets are not relevant because they are specific to T-sheet analysis. This study will use satellite images acquired during the winter season. Thus, in addition to removing Ec and Ets, Es will also be omitted. Since the high water line (HWL) will be used as the shoreline indicator instead of the low water mark (LWM), Etd will also be removed. The equation below will be used to calculate the uncertainty for each extracted shoreline:

$$Ut = \pm \sqrt{(Ed^2 + Ep^2 + Er^2)} \quad (4)$$

2.3.12. Change Rate Calculation

After determining the uncertainty for each shoreline, we will create transects spaced 100 m apart. The rate of change will be determined using linear regression rate (LRR) statistical analysis. The final output will be that of maps displaying areas of erosion and accretion with distinct colour coding.

3. Results and Discussions

3.1. Change in Total Shoreline Length

The objective of the research is to identify and measure the total change in shoreline length. Table 2 shows a total increase of 70,093 m of shoreline between 1982 and 2018. Over 20 years, from 1982 to 2002, there was approximately 11,432 m of new shoreline, accounting for about 571 m of new shoreline per year. The construction of Lusail City started near the shoreline in 2007 and the construction of an artificial island called The Pearl started near Lusail City in 2004. Both Lusail City and The Pearl added 25 km and 31 km of new shoreline, respectively. Both areas contributed to a significant increase of 61,552 m from 2002 to 2013. From 2013 to 2018, there was a minor decrease of 2890 m, constituting a total length of 135,641 m in 2018 (Table 3). This is about a 0.023% decrease in the shoreline

length from 2013 to 2018. Other segments have a smaller change in the shoreline length in comparison to these two segments. A detailed analysis of shoreline changes is presented for each segment.

Table 3. Shoreline length of the study area.

Date (mm/dd/yyyy)	Shoreline Length (Meters)
10/11/1982	65,547
10/17/1992	70,044
8/2/2002	76,979
5/4/2013	138,531
10/9/2018	135,641

3.1.1. Segment A

The United States Geological Survey (USGS) developed a GIS-based system, namely DSAS, for monitoring shoreline changes. Segment A of the study area, which is located in Lusail City, has experienced significant coastal land accretion due to shoreline construction. The components of DSAS include baselines (starting points of all transects), historical shorelines (for the studied periods), DSAS transects (casting from the baseline and intersecting the multiple shoreline features), measurement points, measurement distances, and shoreline uncertainty (set up as a Personal Geodatabase in DSAS). The distance between two neighbouring transects is 100 m and the DSAS transects are 7500 m long. DSAS cast transects orthogonal to the onshore baseline at 100 m intervals to examine the shoreline changes of five timelines on the x-axis (Figure 6). To analyse accretion, data from transects 61, 62, and 63 are analysed (Figure 7), and to analyse erosion, data from transects 14, 15, and 16 are used. The total change in the shoreline length in this segment is also analysed to fully understand the shoreline changes (Figure 8).

The three transects display similar land accretion patterns (Figure 6). The linear regression rates of transects 61, 62, and 63 are 20.1 m/y, 19.86 m/y, and 18.1 m/y, respectively. This means that the average land growth rate over the past 36 years is about 18.1 m/y to 20.1 m/y. However, there was 250 m to 350 m of coastal erosion from 1982 to 2002. The transects in Figure 6 are colour-coded, with green showing a land gain and red showing a land loss. Land accretion started with the construction of Lusail City in 2006, leading to an increase of 855 m in 7 years (Figure 8). From 2013 onwards, the shoreline has remained stable on the northern side of Segment A, but there was a significant shift towards land on the southern side from 2013 to 2018.

Transects 14, 15, and 16 demonstrate a coastal land loss from 2013 to 2018. The shoreline change in this area is unusual, with a land loss of 360 m to 370 m from 1982 to 2002, followed by 735 m of accretion in the next 11 years, and a reduction of 895 m from 2015 to 2018. This pattern is not limited to the three transects, but rather applies to the entire southern part of Lusail City (Figure 9). Visual interpretation of satellite maps suggests that the area was not affected by erosion, but rather that the entire landmass was submerged under water.

To understand shoreline changes, analysing changes in shoreline length over time is crucial. In Lusail City, the length of the shoreline fluctuated from 7624 m to 6801 m from 1982 to 2002 (Table 4). The construction of Lusail City started in 2006, causing the shoreline length to increase fourfold to 24,443 m by 2013. From 2013 to 2018, the shoreline length remained largely unchanged. However, the increase in length did not result in a significant increase in the shoreline area due to the complex construction pattern in the northern part of the city (Figure 9). Currently, the shoreline of Lusail City is unstable due to coastal construction, and further changes are expected in the near future. A field survey completed on 2 April 2019 showed ongoing coastal construction (Figure 10).

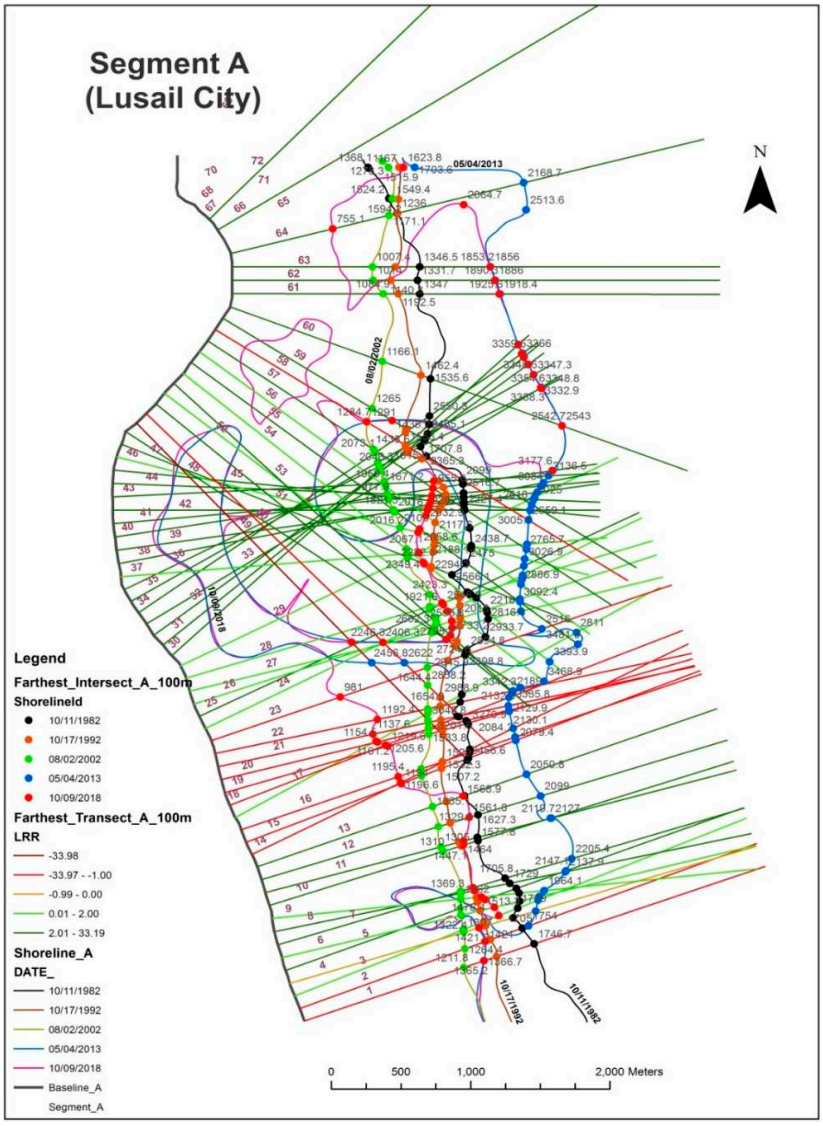

Figure 6. Shoreline map of Segment A.

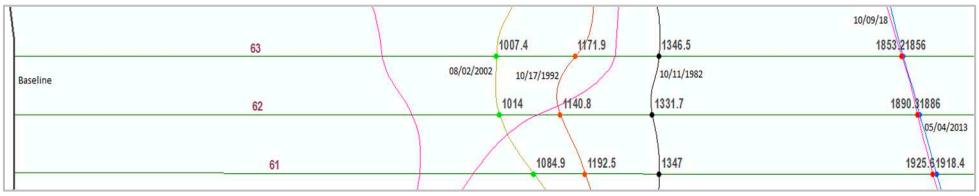

Figure 7. Transects 61, 62, and 63 of Segment A.

Table 4. Total change in shoreline length.

Date	Shoreline Length (m)
10/11/1982	7624
10/17/1992	6897
8/2/2002	6801
5/4/2013	24,439
10/9/2018	24,953

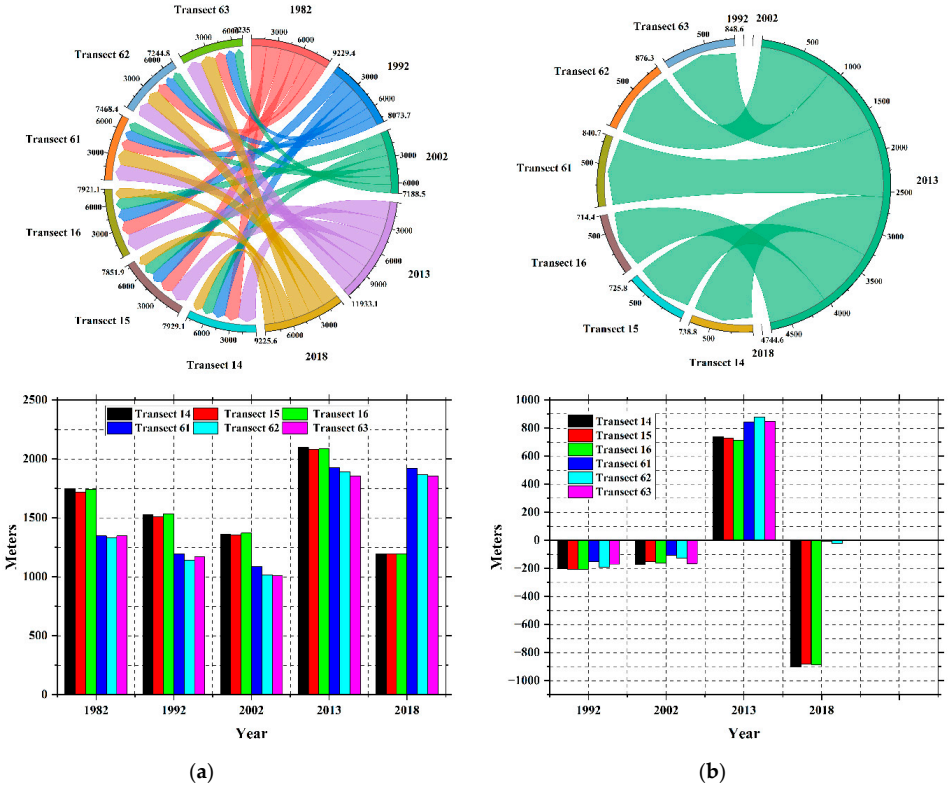

(**a**) (**b**)

Figure 8. (**a**) Distance from baseline (m), (**b**) shoreline gain/loss in comparison to the last timeline (m).

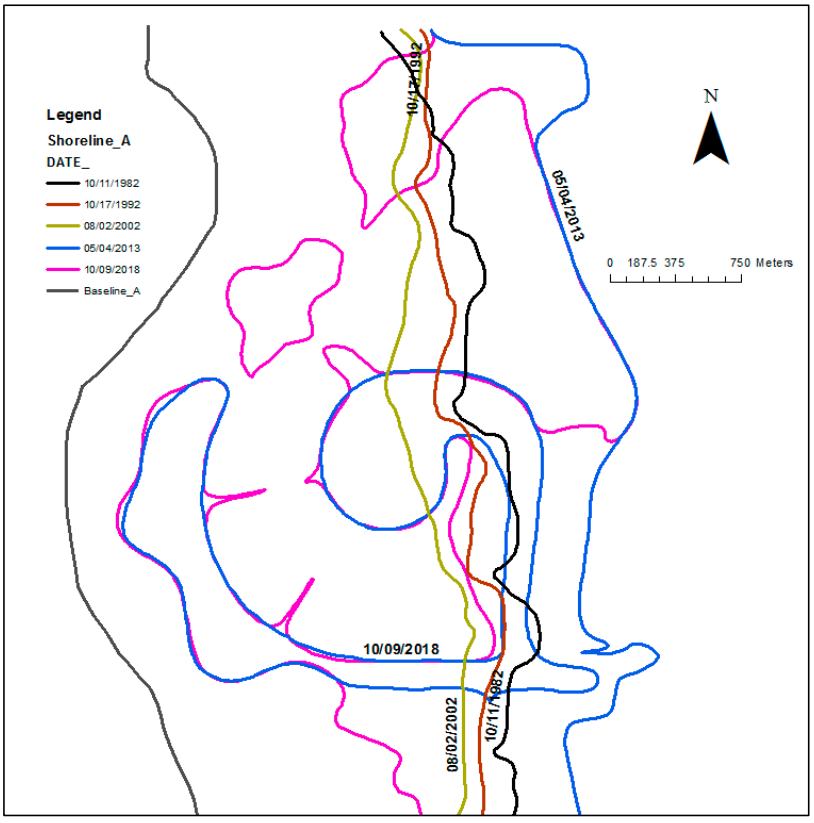

Figure 9. Northern part of Lusail City.

Figure 10. Ongoing coastal construction in Lusail City.

3.1.2. Segment B

Segment B in the study area encompasses The Pearl, Leqtaifiya, and Al Qassar (Figure 11). The construction of The Pearl has resulted in a high gain of coastal land in this segment. Thirty-five transects were drawn at 100 m intervals along the baseline to intersect the five shorelines on the x-axis. To analyse shoreline changes, the shoreline length data of Segment B were obtained from GIS ArcMap (Table 5). The data of transects 21, 20, and 5 were obtained to understand shoreline gains and losses in Segment B (Figure 12).

Table 5. Shoreline length data of Segment B.

Date	Shoreline Length (m)
10/11/1982	4123
10/17/1992	3964
8/2/2002	5742
5/4/2013	36,658
10/9/2018	35,903

Table 5 shows the shoreline lengths of Segment B for each of the five timelines in the study. In 1982, the length was 4123 m, but it increased by 1619 m over the next 20 years. The construction of The Pearl, a manmade island off the coast of the city, resulted in a sevenfold increase in the shoreline length to 36,658 m in 2013 (Figure 12). The Pearl Project created 30 km of new shoreline over the course of 5 years, starting in 2004. The data show a 30,161 m increase in the shoreline length since 2002. The shoreline did not experience significant changes from 2013 to 2018, with an overall change variation of about −700 m.

Three transects were selected from Segment B to analyse the shoreline change patterns. All transects are 5750 m in length. Transects 21 and 20, which are continuous and intersect The Pearl, show a similar change pattern (Figure 12). There was a land loss of approximately 160 m from 1982 to 1992 for both transects. However, shoreline accretion increased to over 320 m in the following 10 years. From 2002 to 2013, the construction of the offshore island, The Pearl, led to a 5.5 km increase in the shoreline length. This massive project resulted in 400 ha of offshore land reclamation and the construction of shoreline protection structures. In contrast, no construction took place in transect 5, located in the southern part of Segment B, leading to minor shoreline changes. A land loss of approximately 200 m was observed over the 36-year study period, with the majority of the loss (230 m) occurring in the early years, as well as 50 m accretion from 1992 to 2002. Overall, Segment B showed high accretion, with minor portions experiencing a land loss at rates ranging from −1 m/y to 7.59 m/y.

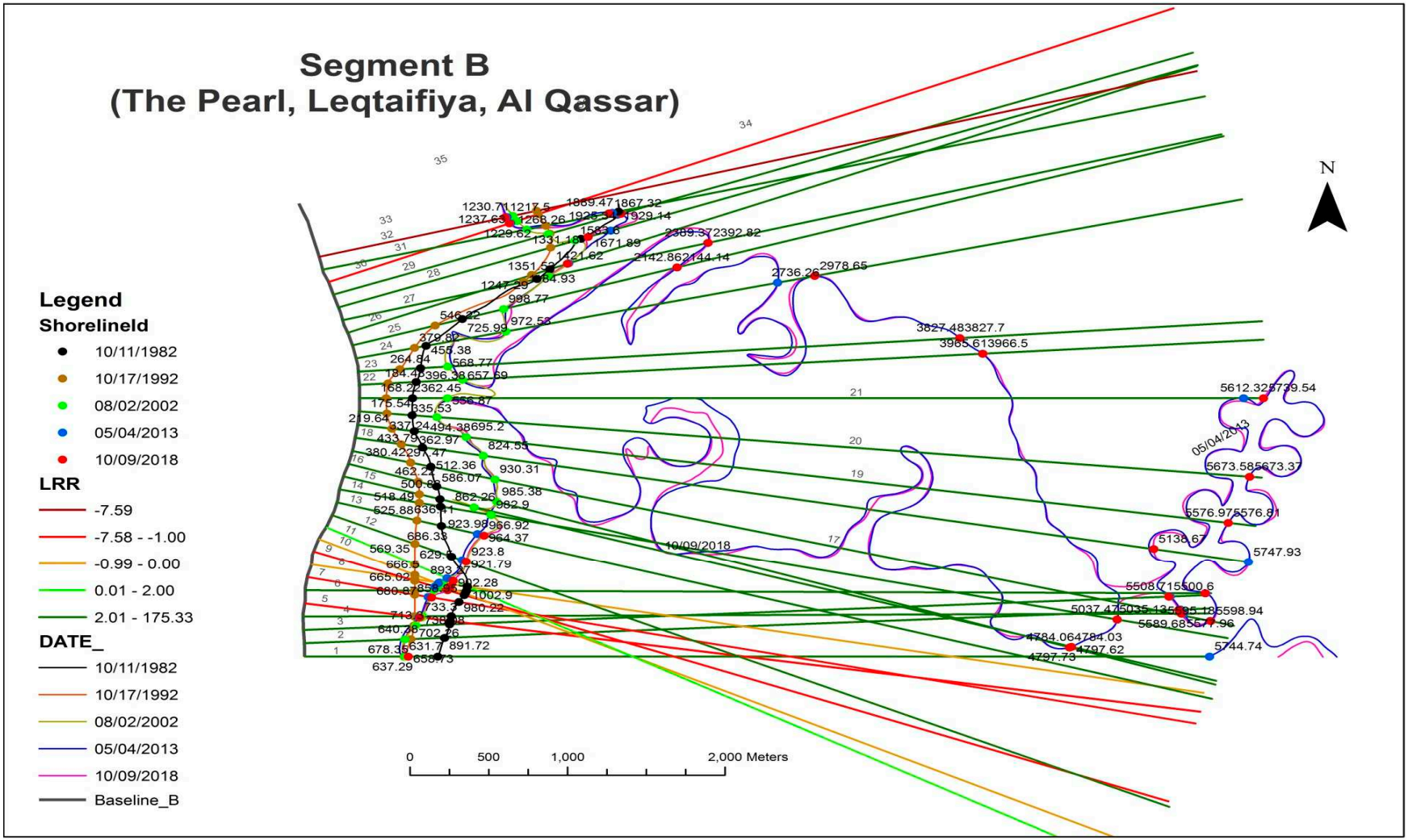

Figure 11. Shoreline map of The Pearl, Leqtaifiya, and Al Qassar area.

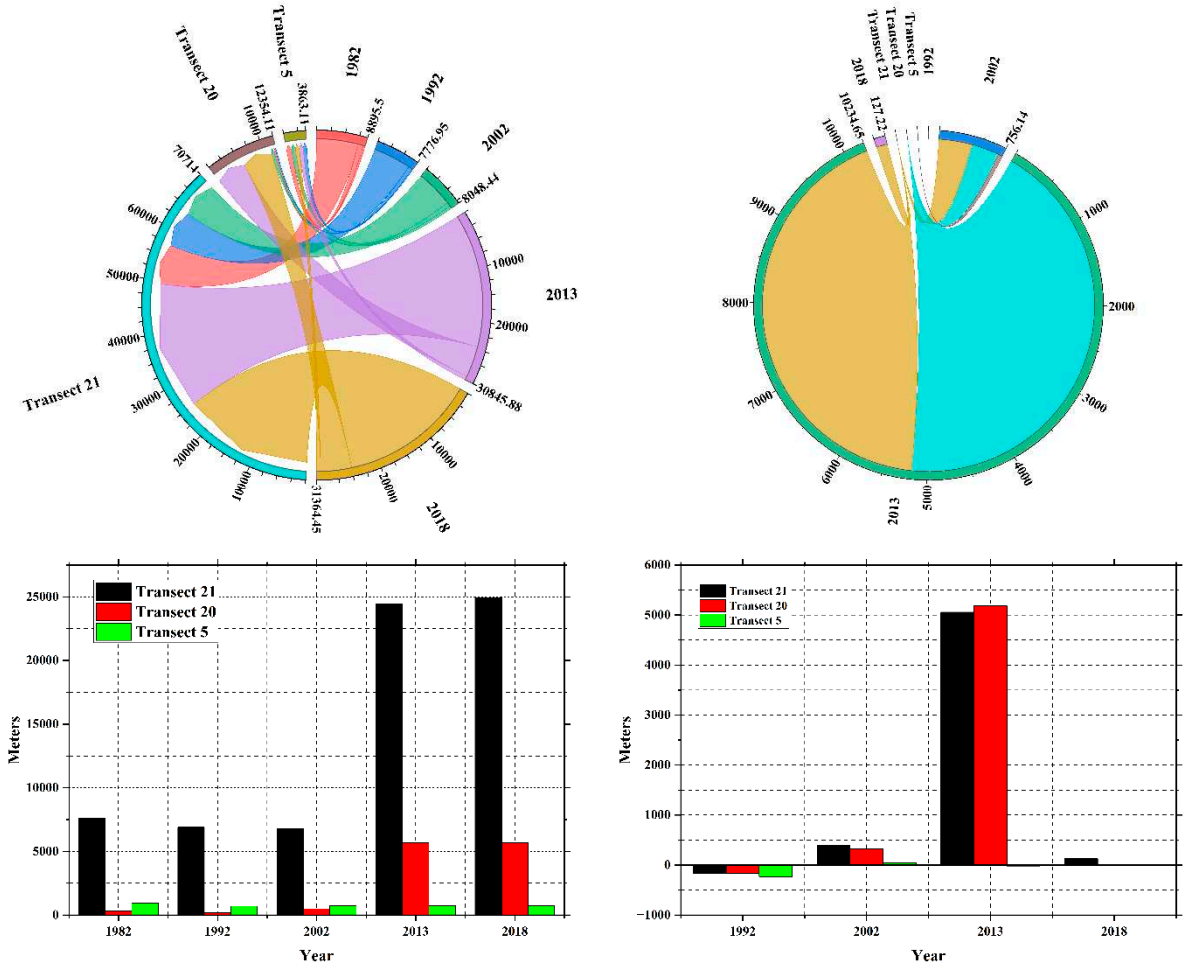

Figure 12. (**a**) Distance from baseline (m), (**b**) shoreline gain/loss in comparison to the last timeline (m).

3.1.3. Segment C

Segment C mostly covers Al Dafna and a small part of Al Qassar in the north. It experienced shoreline change rates ranging from −3.64 m/y to 24.86 m/y, with accretion in the north and erosion in the south, resulting in an overall shoreline loss of 1075 m over the past 36 years (Table 6). To analyse the shoreline changes, four transects (41, 42, 10, and 11) were selected and a field survey was conducted on 3 April 2019 for validation. Transects 41 and 42 (Figure 13) show accretion (green), and transects 10 and 11 (Figure 14) show erosion (red). The field survey confirmed the presence of a sandy beach on the northern side and a protective shoreline on the southern side (Figure 15).

Table 6. Shoreline length data of Segment C.

Date	Shoreline Length (m)
10/11/1982	6726
10/17/1992	6939
8/2/2002	7061
5/4/2013	6599
10/9/2018	5651

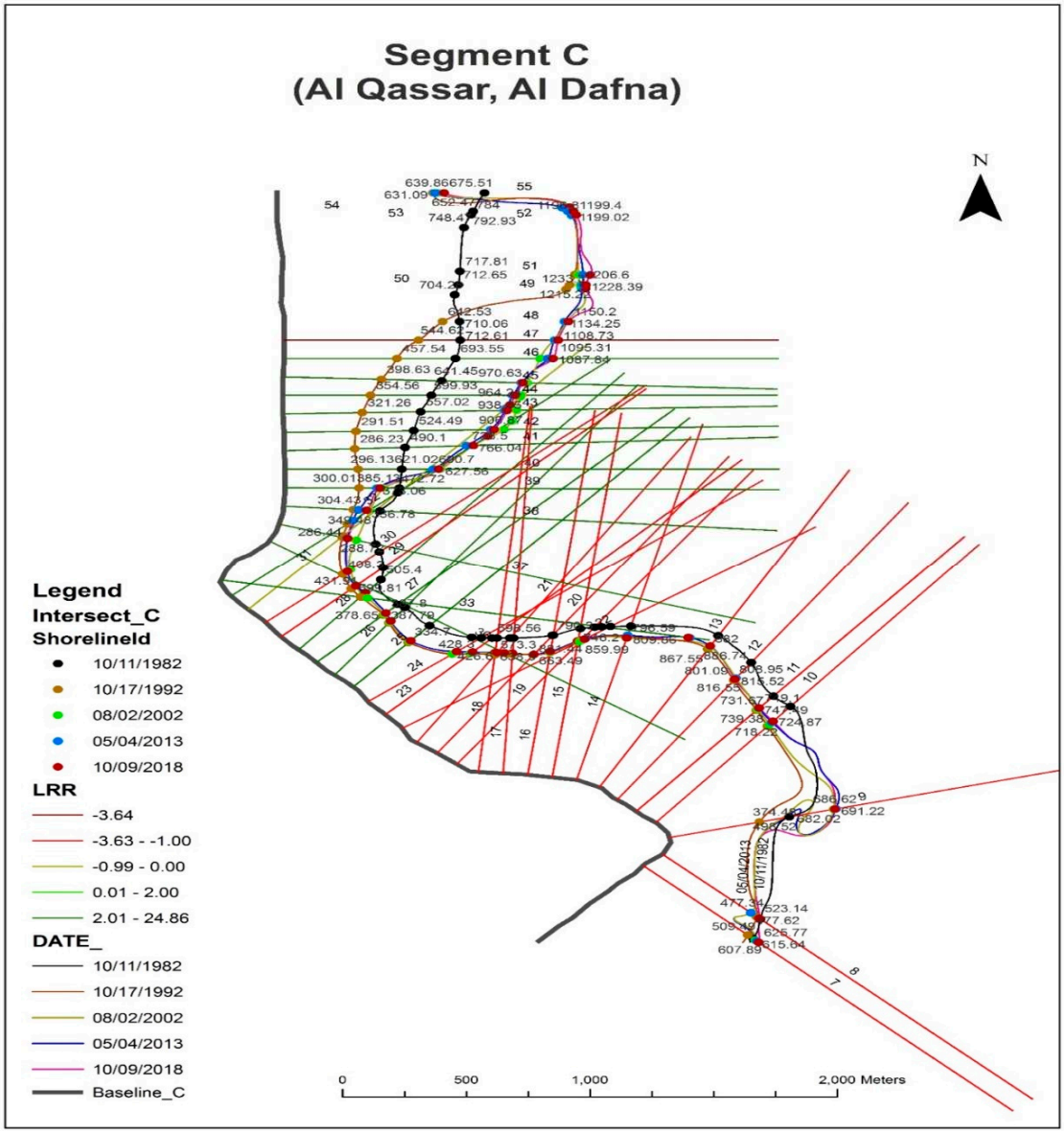

Figure 13. Shoreline of Al Qassar and Al Dafna area.

Segment C underwent over 200 m of shoreline erosion or submergence from 1982 to 1992. However, it recovered 480 to 600 m of land towards the sea over the next decade. The shoreline has been stable since 2002, with changes ranging from ±1 m to 50 m. Analysis of the shoreline distance data reveals that the green-coloured transects had similar shoreline changes to those of transects 41 and 42. Transects 10 and 11 also witnessed a significant shoreline loss from 1982 to 1992, with a high erosion rate of −12.24 m/y. Since 1992, there has been a low accretion rate of 0.67 m/y to 1.29 m/y. From 1992 to 2018, land recovery was less than 50 m, while the land erosion from 1982 to 1992 exceeded 100 m. The red-coloured transects exhibited similar shoreline change patterns to those of transects 10 and 11. Unlike Lusail City and The Pearl, Al Dafna's shoreline has declined by roughly 800 m over the past 36 years. There was 300 m of shoreline accretion from 1982 to 2002, followed by 1600 m of shoreline erosion over the next 16 years. Despite the overall land reduction, the rate of change is relatively low, making Al Dafna's shoreline moderately stable when viewed on a larger scale.

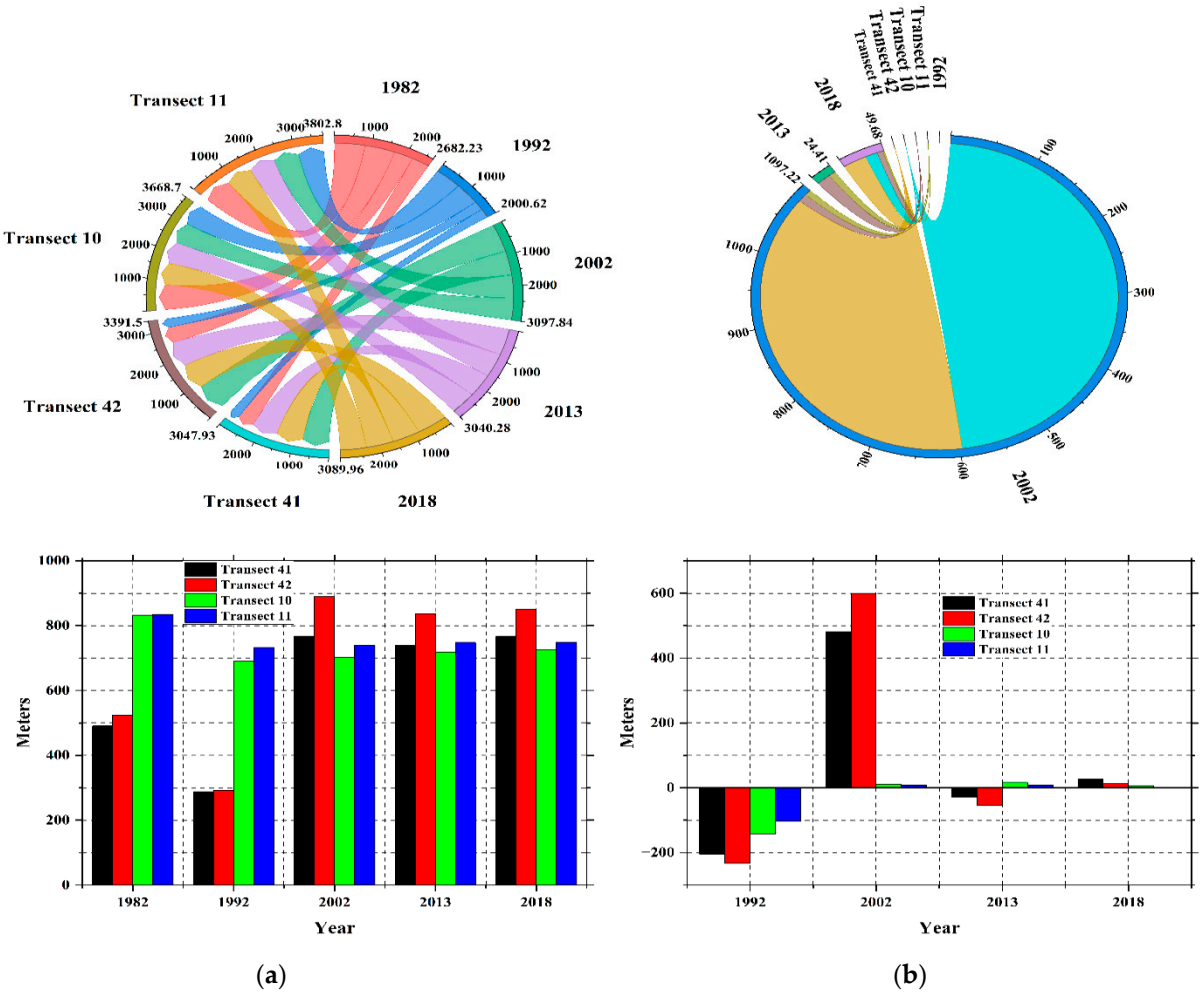

Figure 14. (**a**) Distance from baseline (m), (**b**) shoreline gain/loss in comparison to the last timeline (m).

Figure 15. Shorelines of Segment C.

3.1.4. Segment D

Segment D covers a small part of Al Dafna, Al Corniche, Al Souq, and Doha Port. The most notable shoreline change is in the southeast, driven by the expansion of Doha Port as well as coastal construction projects. Since 1982, 6 km of new shoreline has been created, with 4 km created from 1992 to 2002, and 1 km created since 2002 (Table 7). Ongoing land reclamation near Doha Port is expected to cause minor shoreline changes in the future

(Figure 16). In the north, shoreline protection structures were built in the 1990s, resulting in a stable shoreline with a change rate of ±1.5 m/y (Figure 17).

Table 7. Shoreline length data of Segment D.

Date	Shoreline Length (m)
10/11/1982	11,586
10/17/1992	12,659
8/2/2002	16,628
5/4/2013	17,788
10/9/2018	17,638

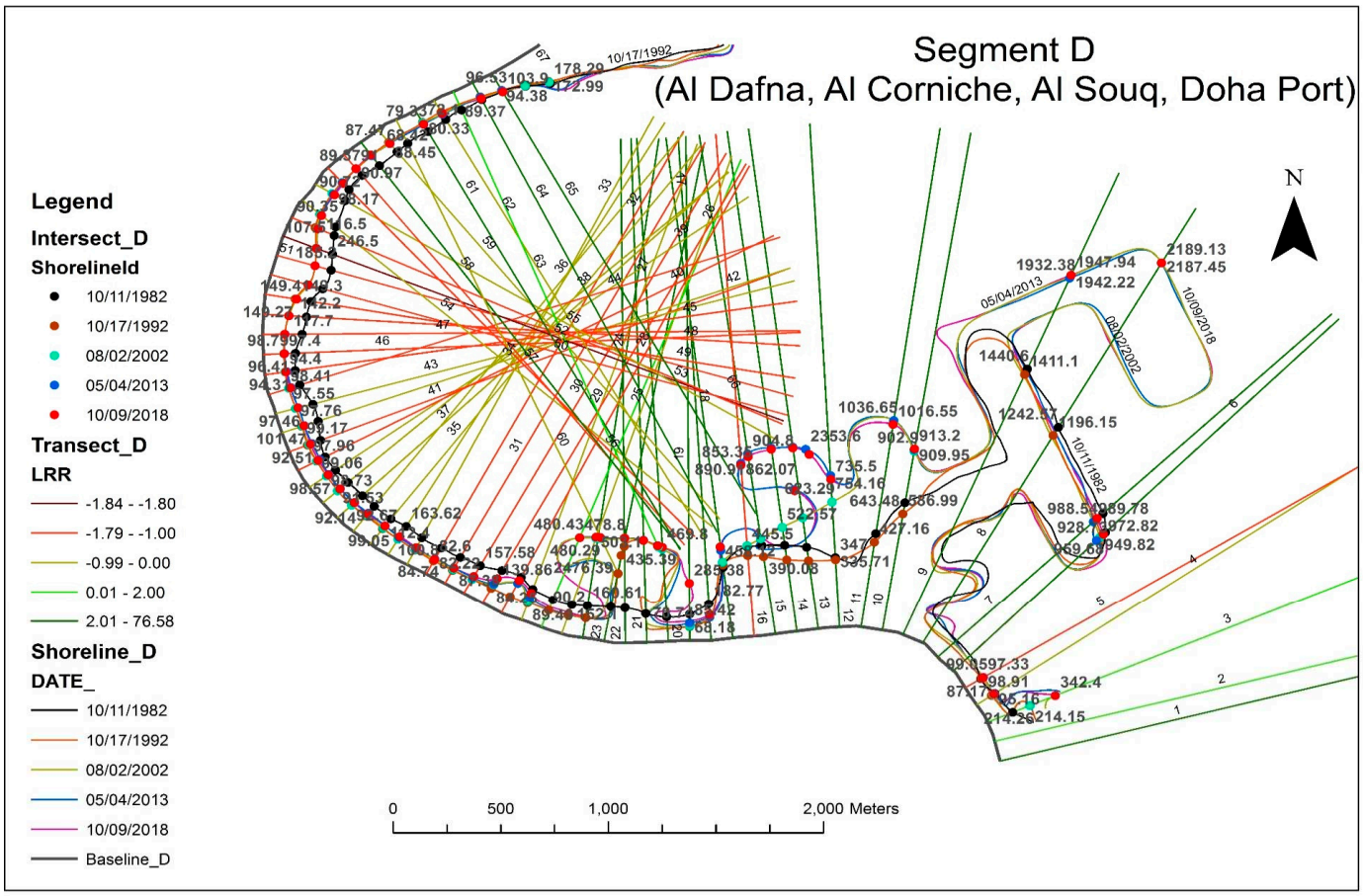

Figure 16. Shoreline of Al Dafna, Al Chorniche, Al Souq, and Doha Port.

(**a**)

(**b**)

Figure 17. (**a**) Protective shorelines of Al Corniche (Segment D), (**b**) ongoing land reclamation near Doha Port.

3.1.5. Segment E

Segment E encompasses Al Khulaifat, Ras Bu Abboud, and Hamad International Airport, and has experienced significant shoreline expansion due to land reclamation for coastal construction (Figure 18). Hamad International Airport alone, occupying 29 km^2, was built with 62 million cubic metres of land reclaimed from the Arabian Gulf, accounting for over 60% of the airport's total area. The project created a new shoreline, estimated at 6311 m, and caused a shoreline movement of 800 to 2600 m towards the sea (Table 8). Other areas in Segment E have shown little change over time. Between 2002 and 2013, 5683 m of new shoreline was created, but 1455 m was reduced between 2013 and 2018 due to land reclamation near the airport's northern side. Land reclamation generally increases the shoreline length, but in this case, a bay was closed with landfill, resulting in a smaller straight shoreline (transect 66 of Figure 15).

Table 8. Shoreline length data of segment E.

Date	Shoreline Length (m)
10/11/1982	13,460
10/17/1992	14,825
8/2/2002	15,543
5/4/2013	21,226
10/9/2018	19,771

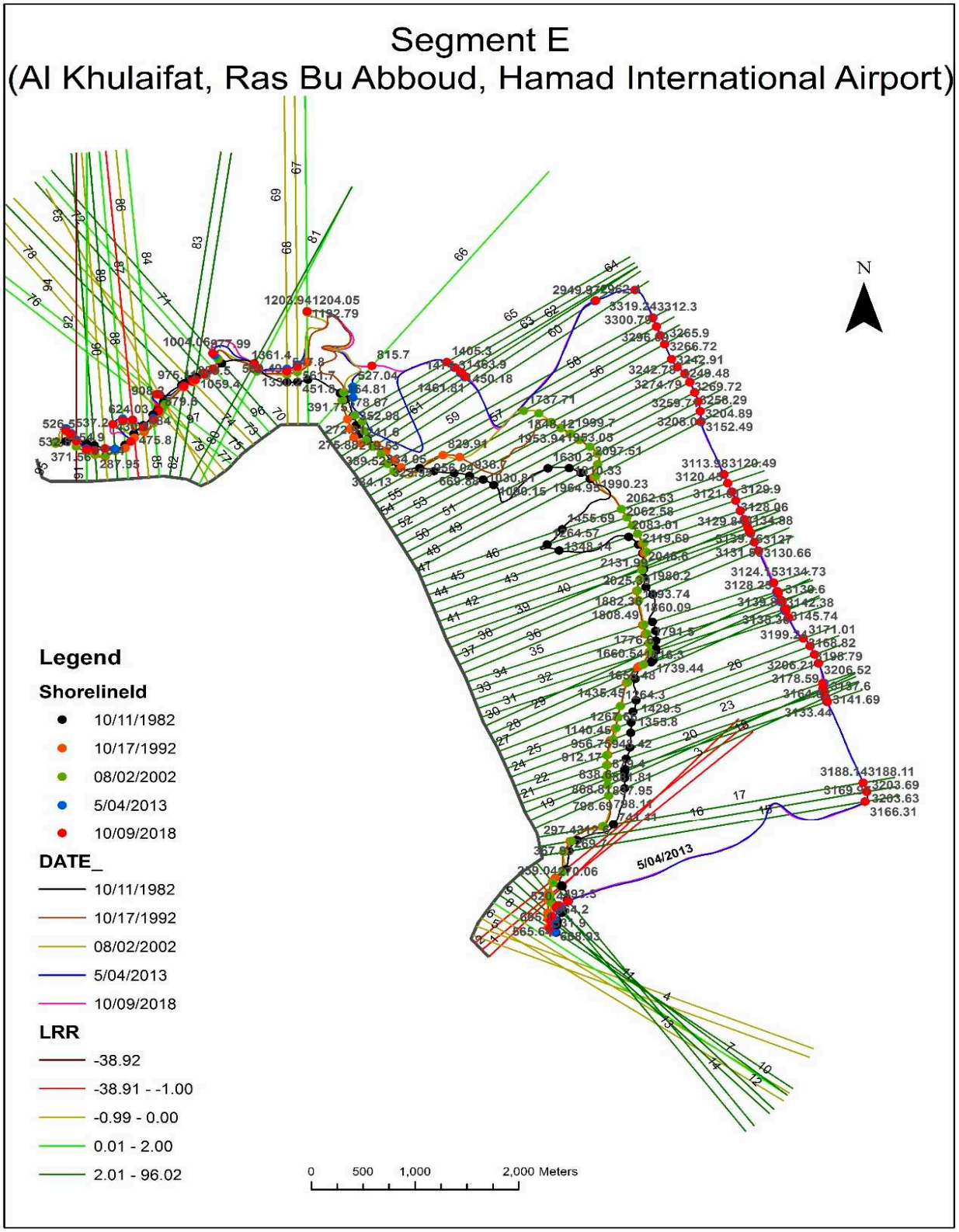

Figure 18. Shoreline of Al Khulaifat, Ras Bu Abboud, and Hamad International Airport.

3.1.6. Segment F

The southern part of Hamad International Airport is occupied by Segment F's shorelines. Of the 46 transects, 14 exhibited a land loss, with a low degradation rate ranging from −2.94 m/y to −0.1 m/y. Meanwhile, the shoreline accretion rate ranges from 11.9 m/y to 0.02 m/y, resulting in an increase of 2320 m in the shoreline length from 1982 to 2018

due to land reclamation for airport construction (Table 9). Transects 8, 28, 39, and 44 were selected to demonstrate shoreline movements, with transect 8 showing land accretion and the others showing erosion from 1982 to 1992 (Figure 19). Transects 39 and 44 experienced a land accretion of 88 m from 1992 to 2013, while the other transects exhibited slow land degradation from 2013 to 2018 (505 m in transect 8). In Segment F, green transects represent land accretion and reclamation, while red transects represent erosion (Figure 20).

Table 9. Shoreline length data of Segment F.

Date	Shoreline Length (m)
10/11/1982	5827
10/17/1992	6588
8/2/2002	6467
5/4/2013	7073
10/9/2018	8147

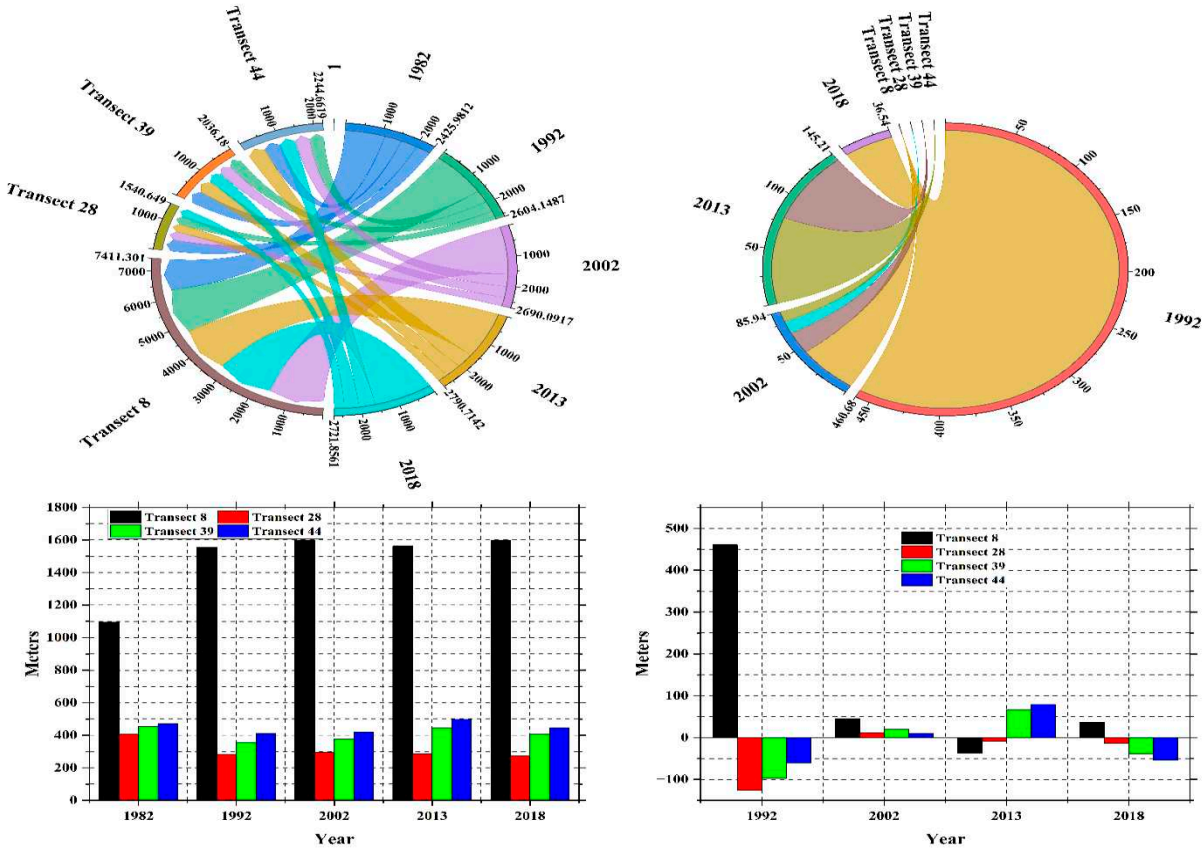

Figure 19. (**a**) Distance from baseline (m), (**b**) shoreline gain/loss in comparison to the last timeline (m).

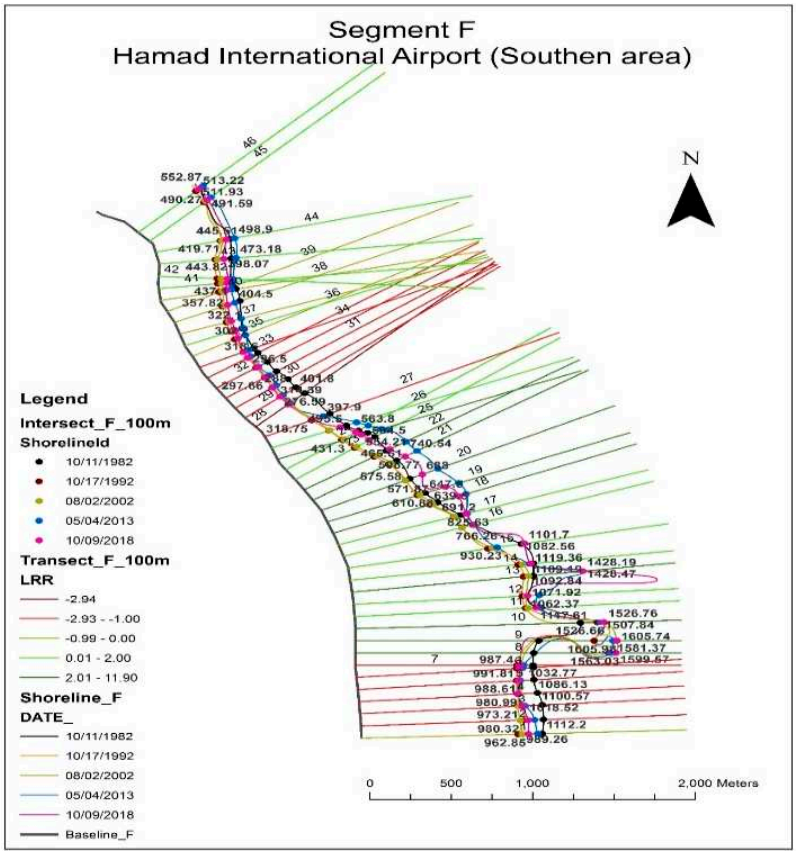

Figure 20. Southern part of Hamad International Airport.

3.1.7. Segment G

Segment G represents the shoreline of Al Wakra City and has experienced a mixed shoreline shift, with change rates ranging from −16.41 m/y to 23.29 m/y. Transects 14 to 16 showed a significant shoreline gain of over 20 m/y after 1992 due to the construction of Al Wakra Fishing Port. Meanwhile, transects 22 to 27 witnessed the highest land erosion at rates higher than −10 m/y. In 1982, the shoreline length was 6163 m, which had slowly increased to 6928 m by 2002 and then rapidly rose to 9726 m in 2013, before decreasing to 8305 m in 2018, resulting in a net increase of 2142 m of shoreline from 1982 to 2018 (Table 10). The increase in shoreline does not necessarily mean overall land accretion, as there can be the erosion and formation of a complex shoreline in a small area. This can be observed in Segment G from transects 19 to 32, where high erosion since 2002 formed a complex shoreline (Figure 21). The northern side of Segment G demonstrated horizontal shoreline accretion, meaning that there was a land gain in terms of area (regardless of coastal length changes).

Table 10. Shoreline length data of Segment G.

Date	Shoreline Length (m)
10/11/1982	6163
10/17/1992	6285
8/2/2002	6918
5/4/2013	9726
10/9/2018	8305

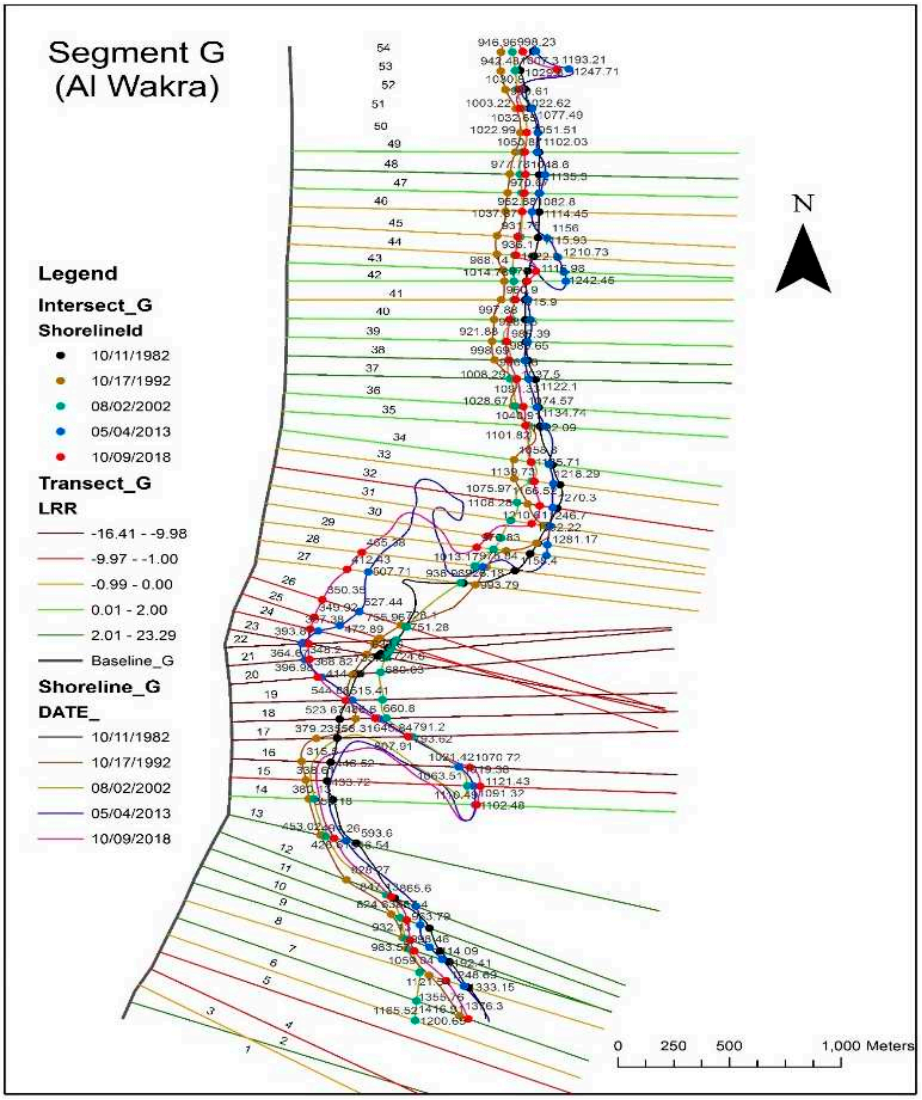

Figure 21. Al Wakra shoreline.

4. Ground Truth Validation

A field survey was conducted to assess the current state of coastal areas and identify the types of shorelines. Two types were found: natural and anthropogenic. Natural shorelines include rocky and sandy beaches, and are impacted by waste disposal and construction material dumping (Figure 22a,b). Anthropogenic shorelines are a result of coastal construction and land reclamation, and are almost all shorelines near coastal cities (mainly Segments A to E) protected by either natural limestone rocks, strategically placed by the shoreline for shoreline stability (Figure 22c), or concrete reinforcement (Figure 22d,e). The survey found natural sandy and rocky beaches in Al Wakra (Segment G) (Figure 22a,b), and manmade sandy beaches in The Pearl (Segment B) and Al Qassar (Segment C). A location map of the survey, with dots representing the survey locations and their coordinates, is presented in Figure 23 and Table 11.

Figure 22. (**a**) Sandy beach in Al Wakra, (**b**) rocky beach in Al Wakra area, (**c**) shoreline protection structure built using natural limestone (Al Wakra Fishing Port), (**d**) protection structure built using concrete reinforcement (Al Corniche), (**e**) protection structure built using concrete reinforcement (Lusail City).

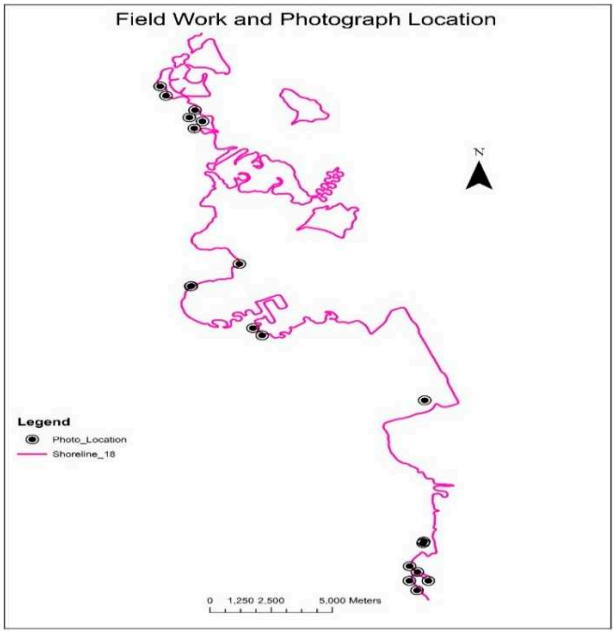

Figure 23. Dot map representing field survey locations.

Table 11. Dates and locations of field survey photos.

Area	Segment	Intersect X	Intersect Y	Date
Lusail City	A	551,585.70	2,810,593.86	4/2/2019
Lusail City	A	551,344.14	2,811,129.38	4/2/2019
Lusail City	A	552,774.44	2,809,771.39	4/2/2019
Lusail City	A	552,535.19	2,809,353.55	4/2/2019
Lusail City	A	552,740.80	2,808,733.45	4/2/2019
Lusail City	A	553,078.78	2,809,131.57	4/2/2019
Al Dafna	C	554,585.82	2,801,014.80	4/2/2019
Al Corniche	D	552,596.02	2,799,735.60	4/2/2019
Al Corniche	D	552,619.10	2,799,749.91	4/2/2019
Doha Port	D	555,142.52	2,797,357.93	4/7/2019
Al Khulaifat	E	555,595.74	2,797,011.74	4/3/2019
Al Khulaifat	E	555,515.31	2,796,939.27	4/3/2019
Hamad International Airport	E	562,163.24	2,793,242.26	4/3/2019
Al Wakra	G	561,849.68	2,782,414.99	4/3/2019
Al Wakra	G	561,537.78	2,782,964.60	4/3/2019
Al Wakra	G	561865.03	2,783,463.17	4/3/2019
Al Wakra	G	561,548.14	2,783,791.44	4/3/2019
Al Wakra	G	562,313.50	2,782,958.56	4/3/2019
Al Wakra	G	562,313.50	2,782,958.56	4/3/2019
Al Wakra	G	562,098.82	2,785,110.62	4/3/2019
Al Wakra	G	562,125.82	2,785,189.09	4/3/2019

5. Discussion

Assessing the impact of anthropogenic evolution on shoreline dynamics is crucial, especially in areas with rapid urbanisation and coastal development such as Qatar. In this study, multi-temporal satellite images were used to assess changes in shoreline dynamics in Qatar and evaluate the impact of natural and anthropogenic activities on these changes. The results of the study show that anthropogenic activities have a significant impact on shoreline dynamics in Qatar. Analysis of the multi-temporal satellite images revealed that the shoreline has undergone significant changes over the last few decades, with the most notable changes occurring in areas with high levels of human activity. The study highlights that coastal development, land reclamation, and dredging have led to significant

alterations in the shoreline dynamics. The construction of artificial islands and other coastal infrastructure has disrupted sediment transport and caused erosion in some areas, while leading to sedimentation in others. These findings suggest that the need for economic development and urbanisation must be balanced with the need to protect the coastal environment. The use of multi-temporal satellite images in this study allowed for a detailed assessment of the changes in shoreline dynamics over time.

The findings of this study have important implications for the management and conservation of coastal ecosystems in Qatar. They suggest that effective management of human activities is necessary to mitigate the impacts on the shoreline and maintain the health and resilience of the ecosystem. Additionally, this study highlights the importance of continued monitoring of shoreline dynamics by means of multi-temporal satellite images to assess the effectiveness of management efforts. The assessment of the impact of anthropogenic evolution on shoreline dynamics in Qatar via multi-temporal satellite images provides valuable insights into the complex interactions between human activities and natural processes in coastal environments. This study underscores the need for a balanced approach to coastal development as well as the importance of effective management practices in maintaining the health and resilience of coastal ecosystems.

5.1. Long-Term Shoreline Changes

Analysis of the long-term changes (1982–2018) along the shoreline of Qatar showed that there was a shift of around 70 km of shoreline towards the seaward side (accretion). This increase is mainly due to coastal construction and land reclamation, particularly the construction of Pearl Island and Lusail City. In contrast, some shoreline areas witnessed shifting in the landward direction (erosion). However, the degree of erosion is low and completely influenced by natural actions, mainly due to the low impact of the atmospheric process in this region, such as the wind and associated wave motions. These results can also be explained by the low sea level oscillations because of climate change and the absence of tectonic phenomena in this region. In general, analysis of the long-term shoreline changes revealed that the study area experienced an annual accretion rate of 1.95 km. This rate is very high when compared with results from other studies. For example, the average annual increase rate on the João Pessoa shoreline was 0.55 m [14]. This difference is mainly attributed to the causes of this increase, as in our study area, the increase is related to anthropogenic evolution, while in João Pessoa, it is due to natural processes.

5.2. Short-Term Shoreline Changes

The analysis of short-term shoreline changes was based on dividing the study area spatially and temporally. Spatially, the study area was divided into seven segments along the coastal area, from Lusail City in the northern part of Doha (the capital city of Qatar) to Al Wakra City (which is to the south of Doha). Temporally, the analysis was conducted for five different intervals of 5–11 years. The differences in time intervals were due to the availability of the Landsat images for the study period. The five different time intervals were 1982–1992, 1992–2002, 2002–2013, and 2013–2018. This short-term assessment is important in understanding episodic shoreline movements as well as responses to geomorphic, human, and natural processes [87,88]. The analysis revealed variations in accretion and erosion between the segments and within the transects during these periods. The main differences are due to land reclamation and coastal development, with some of these segments witnessing more development than the others, particularly over the last two time periods. In addition, some accretion was due to natural sediment accumulation, such as in the southern parts of the study area in Al Wakra and on the southern side of HIA.

The outcomes of this study align with the outcomes of other studies and vary from other studies conducted regionally and internationally. Regionally, Alharbi et al. [89] investigated the shoreline dynamics in the Jizan area in Saudi Arabia between 1973 and 2011 using Landsat imagery and inter-survey methods. They found shoreline changes including a maximum accretion of 36.4 m and maximum erosion of 12.9 m. These shoreline

changes are mainly due to anthropogenic evolution such as infrastructure development, land reclamation, and port development and some natural processes such as spit formations and valley outfalls. Daoudi1 and Niang [90] investigated the shoreline changes along the coast of Jeddah in Saudi Arabia between 1951 and 2018 using DSAS, linear regression rate (LRR), and end point rate (EPR) for the statistical analysis. They found accretion trends, particularly around the port in the central city, where the maximum accretion rate was 47.6 m/year with an average rate of 17.8 m/year. This high accretion rate is due to land reclamation, particularly the continuous expansion of Jeddah port, where 23 km^2 of sea and islets was backfilled for port facilities. Niang [91] investigated the shoreline changes in the Yanbu coastal zone in Saudi Arabia between 1965 and 2019 using DSAS, weighted linear regression (WLR), end point rate (EPR), net shoreline movement (NSM), and linear regression rate (LRR) statistical methods as well as multi-temporal satellite data. They found a maximum accretion of 1655.9 m and a maximum erosion of 1484.8 m. These changes in shoreline morphology were mainly due to human activities, as an area of around 20 km^2 of sea islets has been dug up or backfilled for different purposes. Al-Zubieri et al. [92] examined the shoreline dynamics along the Red Sea coast between Al Lith and Ras Mahasin in Saudi Arabia between 1984 and 2018 using medium-resolution satellite imagery, tasseled cap transformation, EPR, LRR, NSM, and LMS. They found that the accretion and erosion patterns along the shoreline related mainly to natural processes such as wave action and the littoral drift of sediments by longshore currents. The erosion and accretion areas exceeded 12.3 and 0.89 km^2, respectively. Aldogom et al. [93] investigated the shoreline dynamics in the United Arab Emirates (UAE) over a period of 47 years using DSAS, LRR, ERP, and net shoreline movement (NSM). They found accretion and erosion patterns, where the accretion took place near urban areas due to land reclamation. The erosion rate was recorded as 10.01 m/year while the accretion rate reached 10.2 m/year. Aladwani [94] investigated the shoreline dynamics in Kuwait between 1986 and 2021 using DSAS, EPR, and LRR. The study found that erosion is the main pattern that affects the shoreline change, and this process was due to natural causes.

On the international scale, many studies have been conducted in different parts of the world. Esmail et al. [3] investigated the shoreline dynamic of Damietta city in Egypt between 1990 and 2015 using DSAS, EPR, and LRR statistical methods. They found both accretion and erosion patterns, where the accretion rate was between 10 and 12 m/year while the erosion rate was −78 m/year. These changes are due to wave and current effects. Jonah et al. [95] studied the shoreline change in three neighboring coastal communities in the Central Region of Ghana between 1974 and 2012, and recorded erosion at a rate of -1.24 m/year^{-1} due to human activities, mainly due to exploitation of large amounts of sand and stones to use them in the construction industry. Duru [1] investigated the shoreline changes along Lake Sapanca in Turkey using DSAS between 1975 and 2016. The shoreline underwent accretion during the study period at a rate of 2.7 m/year, mainly due anthropogenic activities such as extracting freshwater from the lake, the deposition of sediments, and cyclic variation in rainfall.

6. Conclusions

This study aimed to examine 40-year shoreline changes along the east coast of Qatar by means of the normalised difference vegetation index and tasselled cap transformation techniques for shoreline extraction. The Digital Shoreline Analysis System tools and linear regression rate statistics revealed significant shoreline changes, primarily due to land reclamation and coastal construction without protective measures. The study period witnessed the creation of 60 km of new shoreline, mostly from 2002 to 2013. These human-induced developments started after 2002 and some are ongoing.

Assessing the impact of anthropogenic evolution and natural processes on shoreline dynamics is a critical area of research that is becoming increasingly important in facing climate change and its impacts on coastal communities. In this study, multi-temporal satellite images were used to assess the changes in shoreline dynamics over time, taking

into account both natural processes and anthropogenic activities. The results of the study indicate that both natural processes and anthropogenic activities have a significant impact on shoreline dynamics. Analysis of the multi-temporal satellite images revealed that land reclamation, coastal construction, erosion, sedimentation, and other anthropogenic and natural processes play a significant role in shaping the shoreline over time.

Moreover, the study highlights the importance of using multi-temporal satellite images in assessing shoreline dynamics. By comparing images taken over different periods, we were able to identify and quantify changes in the shoreline, including in the shoreline width. One of the key findings of this study was the significant impact of anthropogenic activities on shoreline dynamics. The analysis revealed that coastal development was the primary driver of changes in the shoreline. These findings highlight the importance of balancing the need for economic development with the need to protect the shoreline and the environment. What is more, this study points to the potential of multi-temporal satellite images as a tool for monitoring and managing the shoreline. By providing a comprehensive view of shoreline dynamics over time, these images can help to identify areas at risk of erosion or other changes, as well as supporting efforts to manage and mitigate the impacts of natural processes and human activities. Overall, the assessment of the impact of anthropogenic evolution and natural processes on shoreline dynamics by means of multi-temporal satellite images provides valuable insights into the complex and dynamic nature of coastal environments. This study highlights the importance of understanding and managing the interactions between natural processes and human activities in order to protect the shoreline and the communities that depend on it.

One of the limitations of this study is the lack of long-term wave buoy data, tidal currents, and other contemporary hydrodynamic and sediment transport data. The absence of such data limits the capability of investigating the impacts of natural processes on shoreline morphology change.

Author Contributions: Conceptualization, P.B. and A.A.; methodology, P.B. and A.A. and T.A.K.K.; validation, P.B., A.A. and T.A.K.K.; data curation, P.B. and T.A.K.K.; writing—original draft preparation, A.A. and P.B.; writing—review and editing, A.A. and P.B. All authors have read and agreed to the published version of the manuscript.

Funding: This research was funded by Qatar University, High-Impact Grant (No. 211).

Data Availability Statement: No new data were created or analyzed in this study. Data sharing is not applicable to this article.

Acknowledgments: This publication was made possible by a High-Impact Grant award [211] from the Qatar University. The statements made herein are solely the responsibility of the authors. The open access publication of this article was funded by the Qatar National Library (QNL).

Conflicts of Interest: The authors declare no conflict of interest.

References

1. Duru, U. Shoreline change assessment using multi-temporal satellite images: A case study of Lake Sapanca, NW Turkey. *Environ. Monit. Assess.* **2017**, *189*, 385. [CrossRef] [PubMed]
2. Selvan, S.C.; Kankara, R.S.; Prabhu, K.; Rajan, B. Shoreline change along Kerala, south-west coast of India, using geo-spatial techniques and field measurement. *Nat. Hazards* **2020**, *100*, 17–38. [CrossRef]
3. Esmail, M.; Mahmod, W.E.; Fath, H. Assessment and prediction of shoreline change using multi-temporal satellite images and statistics: Case study of Damietta coast, Egypt. *Appl. Ocean Res.* **2019**, *82*, 274–282. [CrossRef]
4. Patel, K.; Jain, R.; Patel, A.N.; Kalubarme, M.H. Shoreline change monitoring for coastal zone management using multi-temporal Landsat data in Mahi River estuary, Gujarat State. *Appl. Geomat.* **2021**, *13*, 333–347. [CrossRef]
5. Adu–Boahen, K.; Emmanuel, M.A.; Kwaku, K.K.; Osman, A. Socio-Economic Impact of Lake Bosomtwe Shoreline Changes on Catchment Residents in Ghana. *Int. J. Sci. Res. Publ.* **2014**, *4*, 1–7.
6. Paterson, S.K.; O'Donnell, A.; Loomis, D.K.; Hom, P. The Social and Economic Effects of Shoreline Change: North Atlantic, South Atlantic, Gulf of Mexico, and Great Lakes Regional Overview. Available online: https://www.csc.noaa.gov/pub/socioeconomic/NSMS/FourRegionReport/1310484279-FourRegionSocioEconofShorelineChangeFinalReport.July.pdf (accessed on 27 November 2021).

7. Moussa, M.; Baccar, L.; Ben Khemis, R. La lagune de Ghar El Melh: Diagnostic écologique et perspectives d'aménagement hydraulique. *Rev. Des Sci. De L'eau/J. Water Sci.* **2005**, *18*, 13–26. [CrossRef]
8. Guimarais, M.; Zúñiga-Ríos, A.; Cruz-Ramírez, C.; Chávez, V.; Odériz, I.; van Tussenbroek, B.; Silva, R. The Conservational State of Coastal Ecosystems on the Mexican Caribbean Coast: Environmental Guidelines for Their Management. *Sustainability* **2021**, *13*, 2738. [CrossRef]
9. Nichols, C.R.; Zinnert, J.; Young, D.R. Degradation of Coastal Ecosystems: Causes, Impacts and Mitigation Efforts. In *Tomorrow's Coasts: Complex and Impermanent*; Coastal Research Library: Cham, Switzerland, 2018; Volume 27, pp. 119–136. [CrossRef]
10. Lewin, W.-C.; Mehner, T.; Ritterbusch, D.; Brämick, U. The influence of anthropogenic shoreline changes on the littoral abundance of fish species in German lowland lakes varying in depth as determined by boosted regression trees. *Hydrobiologia* **2014**, *724*, 293–306. [CrossRef]
11. Jangir, B.; Satyanarayana, A.N.V.; Swati, S.; Jayaram, C.; Chowdary, V.M.; Dadhwal, V.K. Delineation of spatio-temporal changes of shoreline and geomorphological features of Odisha coast of India using remote sensing and GIS techniques. *Nat. Hazards* **2016**, *82*, 1437–1455. [CrossRef]
12. Hoque, M.A.-A.; Ahmed, N.; Pradhan, B.; Roy, S. Assessment of coastal vulnerability to multi-hazardous events using geospatial techniques along the eastern coast of Bangladesh. *Ocean Coast. Manag.* **2019**, *181*, 104898. [CrossRef]
13. D'Alessandro, F.; Tomasicchio, G.R. Wave–dune interaction and beach resilience in large-scale physical model tests. *Coast. Eng.* **2016**, *116*, 15–25. [CrossRef]
14. Santos, C.A.G.; Nascimento, T.V.M.D.; Mishra, M.; da Silva, R.M. Analysis of long- and short-term shoreline change dynamics: A study case of João Pessoa city in Brazil. *Sci. Total. Environ.* **2021**, *769*, 144889. [CrossRef]
15. Rangel-Buitrago, N.; Neal, W.J.; Bonetti, J.; Anfuso, G.; de Jonge, V.N. Vulnerability assessments as a tool for the coastal and marine hazards management: An overview. *Ocean Coast. Manag.* **2020**, *189*, 105134. [CrossRef]
16. Blackburn, S.; Pelling, M.; Marques, C. Megacities and the Coast: Global Context and Scope for Transformation. In *Coasts and Estuaries: The Future*; Elsevier: Amsterdam, The Netherlands, 2019; pp. 661–669. [CrossRef]
17. Nassar, K.; Mahmod, W.E.; Fath, H.; Masria, A.; Nadaoka, K.; Negm, A. Shoreline change detection using DSAS technique: Case of North Sinai coast, Egypt. *Mar. Georesour. Geotechnol.* **2018**, *37*, 81–95. [CrossRef]
18. Chen, S.-S.; Chen, L.-F.; Liu, Q.-H.; Li, X.; Tan, Q. Remote sensing and GIS-based integrated analysis of coastal changes and their environmental impacts in Lingding Bay, Pearl River Estuary, South China. *Ocean Coast. Manag.* **2005**, *48*, 65–83. [CrossRef]
19. Abulibdeh, A.; Al-Awadhi, T.; Al Nasiri, N.; Al-Buloshi, A.; Abdelghani, M. Spatiotemporal mapping of groundwater salinity in Al-Batinah, Oman. *Groundw. Sustain. Dev.* **2021**, *12*, 100551. [CrossRef]
20. Mishra, M. Geomorphic regionalization of coastal zone using geospatial technology. *Int. J. Environ. Geoinf.* **2016**, *3*, 11–23. Available online: https://dergipark.org.tr/en/pub/ijegeo/article/304479 (accessed on 27 November 2021). [CrossRef]
21. Misra, A.; Ramakrishnan, B. Assessment of coastal geomorphological changes using multi-temporal Satellite-Derived Bathymetry. *Cont. Shelf Res.* **2020**, *207*, 104213. [CrossRef]
22. Aucelli, P.P.C.; Mattei, G.; Caporizzo, C.; Cinque, A.; Troisi, S.; Peluso, F.; Stefanile, M.; Pappone, G. Ancient Coastal Changes Due to Ground Movements and Human Interventions in the Roman Portus Julius (Pozzuoli Gulf, Italy): Results from Photogrammetric and Direct Surveys. *Water* **2020**, *12*, 658. [CrossRef]
23. Baral, R.; Pradhan, S.; Samal, R.N.; Mishra, S.K. Shoreline Change Analysis at Chilika Lagoon Coast, India Using Digital Shoreline Analysis System. *J. Indian Soc. Remote Sens.* **2018**, *46*, 1637–1644. [CrossRef]
24. Roy, S.; Mahapatra, M.; Chakraborty, A. Shoreline change detection along the coast of Odisha, India using digital shoreline analysis system. *Spat. Inf. Res.* **2018**, *26*, 563–571. [CrossRef]
25. Borrelli, M.; Boothroyd, J.C. Calculating Rates of Shoreline Change in a Coastal Embayment with Fringing Salt Marsh Using the 'Marshline', a Proxy-Based Shoreline Indicator. *Northeast. Nat.* **2020**, *27*, 132–156. [CrossRef]
26. Cazenave, A.; Le Cozannet, G. Sea level rise and its coastal impacts. *Earth's Futur.* **2014**, *2*, 15–34. [CrossRef]
27. Bama, V.P.S.; Rajakumari, S.; Ramesh, R. Coastal vulnerability assessment of Vedaranyam swamp coast based on land use and shoreline dynamics. *Nat. Hazards* **2020**, *100*, 829–842. [CrossRef]
28. Maiti, S.; Bhattacharya, A.K. Shoreline change analysis and its application to prediction: A remote sensing and statistics based approach. *Mar. Geol.* **2009**, *257*, 11–23. [CrossRef]
29. Alahmadi, M.; Mansour, S.; Dasgupta, N.; Abulibdeh, A.; Atkinson, P.M.; Martin, D.J. Using Daily Nighttime Lights to Monitor Spatiotemporal Patterns of Human Lifestyle under COVID-19: The Case of Saudi Arabia. *Remote Sens.* **2021**, *13*, 4633. [CrossRef]
30. Fadda, E.H.; Abulibdeh, A.O.; Al Balushi, A.S. Using Geomatics Techniques to Produce a Geospatial Database System for Geological Hazards in the Al-Salt Area. In Proceedings of the ICVISP 2019: 3rd International Conference on Vision, Image and Signal Processing, Vancouver, BC, Canada, 26–28 August 2019. [CrossRef]
31. Al-Hatrushi, S.M. Monitoring of the shoreline change using remote sensing and GIS: A case study of Al Hawasnah tidal inlet, Al Batinah coast, Sultanate of Oman. *Arab. J. Geosci.* **2013**, *6*, 1479–1484. [CrossRef]
32. Vos, K.; Splinter, K.D.; Harley, M.D.; Simmons, J.A.; Turner, I.L. CoastSat: A Google Earth Engine-enabled Python toolkit to extract shorelines from publicly available satellite imagery. *Environ. Model. Softw.* **2019**, *122*, 104528. [CrossRef]
33. Sunder, S.; Ramsankaran, R.; Ramakrishnan, B. Inter-comparison of remote sensing sensing-based shoreline mapping techniques at different coastal stretches of India. *Environ. Monit. Assess.* **2017**, *189*, 290. [CrossRef]

34. Sánchez-García, E.; Palomar-Vázquez, J.; Pardo-Pascual, J.; Almonacid-Caballer, J.; Cabezas-Rabadán, C.; Gómez-Pujol, L. An efficient protocol for accurate and massive shoreline definition from mid-resolution satellite imagery. *Coast. Eng.* **2020**, *160*, 103732. [CrossRef]
35. Kim, H.; Lee, S.B.; Min, K.S. Shoreline Change Analysis using Airborne LiDAR Bathymetry for Coastal Monitoring. *J. Coast. Res.* **2017**, *79*, 269–273. [CrossRef]
36. Tak, W.; Jun, K.; Kim, S.; Lee, H. Using Drone and LiDAR to Assess Coastal Erosion and Shoreline Change due to the Construction of Coastal Structures. *J. Coast. Res.* **2020**, *95*, 674–678. [CrossRef]
37. Yun, K.; Lee, C.K.; He, G.; Park, B.W. Monitoring of Shoreline Change at Chollipo Beach in South Korea. *J. Coast. Res.* **2021**, *114*, 469–473. [CrossRef]
38. Wziątek, D.Z.; Terefenko, P.; Kurylczyk, A. Multi-Temporal Cliff Erosion Analysis Using Airborne Laser Scanning Surveys. *Remote Sens.* **2019**, *11*, 2666. [CrossRef]
39. Shin, B.; Kim, K. Estimation of Shoreline Change Using High Resolution Images. *Procedia Eng.* **2015**, *116*, 994–1001. [CrossRef]
40. Al Fugura, A.; Billa, L.; Pradhan, B. Semi-automated procedures for shoreline extraction using single RADARSAT-1 SAR image. *Estuar. Coast. Shelf Sci.* **2011**, *95*, 395–400. [CrossRef]
41. Kuleli, T. Quantitative analysis of shoreline changes at the Mediterranean Coast in Turkey. *Environ. Monit. Assess.* **2010**, *167*, 387–397. [CrossRef]
42. Dereli, M.A.; Tercan, E. Assessment of Shoreline Changes using Historical Satellite Images and Geospatial Analysis along the Lake Salda in Turkey. *Earth Sci. Inform.* **2020**, *13*, 709–718. [CrossRef]
43. Imamoglu, M.; Kahraman, F.; Cakir, Z.; Sanli, F.B. Ground Deformation Analysis of Bolvadin (W. Turkey) by Means of Multi-Temporal InSAR Techniques and Sentinel-1 Data. *Remote Sens.* **2019**, *11*, 1069. [CrossRef]
44. Ford, M. Shoreline changes interpreted from multi-temporal aerial photographs and high resolution satellite images: Wotje Atoll, Marshall Islands. *Remote Sens. Environ.* **2013**, *135*, 130–140. [CrossRef]
45. Mujabar, P.S.; Chandrasekar, N. Shoreline change analysis along the coast between Kanyakumari and Tuticorin of India using remote sensing and GIS. *Arab. J. Geosci.* **2013**, *6*, 647–664. [CrossRef]
46. Elnabwy, M.T.; Elbeltagi, E.; El Banna, M.M.; Elshikh, M.M.; Motawa, I.; Kaloop, M.R. An Approach Based on Landsat Images for Shoreline Monitoring to Support Integrated Coastal Management—A Case Study, Ezbet Elborg, Nile Delta, Egypt. *ISPRS Int. J. Geo-Inf.* **2020**, *9*, 199. [CrossRef]
47. Srinivasu, U.; Ravichandran, M.; Han, W.; Sivareddy, S.; Rahman, H.; Li, Y.; Nayak, S. Causes for the reversal of North Indian Ocean decadal sea level trend in recent two decades. *Clim. Dyn.* **2017**, *49*, 3887–3904. [CrossRef]
48. Randazzo, G.; Barreca, G.; Cascio, M.; Crupi, A.; Fontana, M.; Gregorio, F.; Lanza, S.; Muzirafuti, A. Analysis of Very High Spatial Resolution Images for Automatic Shoreline Extraction and Satellite-Derived Bathymetry Mapping. *Geosciences* **2020**, *10*, 172. [CrossRef]
49. Zollini, S.; Alicandro, M.; Cuevas-González, M.; Baiocchi, V.; Dominici, D.; Buscema, P.M. Shoreline Extraction Based on an Active Connection Matrix (ACM) Image Enhancement Strategy. *J. Mar. Sci. Eng.* **2020**, *8*, 9. [CrossRef]
50. Abulibdeh, A. Spatiotemporal analysis of water-electricity consumption in the context of the COVID-19 pandemic across six socioeconomic sectors in Doha City, Qatar. *Appl. Energy* **2021**, *304*, 117864. [CrossRef] [PubMed]
51. Abulibdeh, A. Analysis of urban heat island characteristics and mitigation strategies for eight arid and semi-arid gulf region cities. *Environ. Earth Sci.* **2021**, *80*, 259. [CrossRef]
52. Abulibdeh, A. Time series analysis of environmental quality in the state of Qatar. *Energy Policy* **2022**, *168*, 113089. [CrossRef]
53. Abulibdeh, A. Water-energy nexus challenges and opportunities in Qatar. In *Qatar: Political, Economic and Social Issues*; Nova: Hauppauge, NY, USA, 2019; pp. 209–227.
54. Abulibdeh, A. Modeling electricity consumption patterns during the COVID-19 pandemic across six socioeconomic sectors in the State of Qatar. *Energy Strat. Rev.* **2021**, *38*, 100733. [CrossRef]
55. Abulibdeh, A.; Al-Awadhi, T.; Al-Barwani, M. Comparative analysis of the driving forces and spatiotemporal patterns of urbanisation in Muscat, Doha, and Dubai. *Dev. Pract.* **2019**, *29*, 606–618. [CrossRef]
56. Zaidan, E.; Abulibdeh, A. Master Planning and the Evolving Urban Model in the Gulf Cities: Principles, Policies, and Practices for the Transition to Sustainable Urbanism. *Plan. Pract. Res.* **2020**, *36*, 193–215. [CrossRef]
57. Zaidan, E.; Abulibdeh, A.; Alban, A.; Jabbar, R. Motivation, preference, socioeconomic, and building features: New paradigm of analyzing electricity consumption in residential buildings. *Build. Environ.* **2022**, *219*, 109177. [CrossRef]
58. Abulibdeh, A.; Zaidan, E.; Jabbar, R. The impact of COVID-19 pandemic on electricity consumption and electricity demand forecasting accuracy: Empirical evidence from the state of Qatar. *Energy Strat. Rev.* **2022**, *44*, 100980. [CrossRef]
59. Ghofrani, A.; Zaidan, E.; Abulibdeh, A. Simulation and impact analysis of behavioral and socioeconomic dimensions of energy consumption. *Energy* **2021**, *240*, 122502. [CrossRef]
60. Mansour, S.; Alahmadi, M.; Abulibdeh, A. Spatial assessment of audience accessibility to historical monuments and museums in Qatar during the 2022 FIFA World Cup. *Transp. Policy* **2022**, *127*, 116–129. [CrossRef]
61. Zaidan, E.; Abulibdeh, A. Modeling ground access mode choice behavior for Hamad International Airport in the 2022 FIFA World Cup city, Doha, Qatar. *J. Air Transp. Manag.* **2018**, *73*, 32–45. [CrossRef]

62. Al-Awadhi, T.; Abulibdeh, A.; Al-Masri, A.N.; Bin Touq, A.; Al-Barawni, M.; El Kenawy, A.M. Spatial and temporal changes in electricity demand regulatory during pandemic periods: The case of COVID-19 in Doha, Qatar. *Energy Strat. Rev.* **2022**, *41*, 100826. [CrossRef]
63. Abulibdeh, A.; Zaidan, E. Empirical analysis of the cross-cultural information searching and travel behavior of business travelers: A case study of MICE travelers to Qatar in the Middle East. *Appl. Geogr.* **2017**, *85*, 152–162. [CrossRef]
64. Kamranzad, B. Persian Gulf zone classification based on the wind and wave climate variability. *Ocean Eng.* **2018**, *169*, 604–635. [CrossRef]
65. Erftemeijer, P.L.A.; Shuail, D.A. Seagrass habitats in the Arabian Gulf: Distribution, tolerance thresholds and threats. *Aquat. Ecosyst. Health Manag.* **2012**, *15*, 73–83. [CrossRef]
66. Al-Naimi, A.; Karani, G.; Littlewood, J. Effects of Land Reclamation on Marine Life on Doha Coastal Region, State of Qatar. In Proceedings of the ISER 57th International Conference, Dubai, United Arab Emirates, 1–2 June 2017; pp. 54–60.
67. Karama, A. Solar DER Investment for MWANI Qatar Building at Hamad Port. In Proceedings of the International Conference on Civil Infrastructure and Construction (CIC 2020), Doha, Qatar, 2–5 February 2020. [CrossRef]
68. Burt, J.A.; Smith, E.G.; Warren, C.; Dupont, J. An assessment of Qatar's coral communities in a regional context. *Mar. Pollut. Bull.* **2016**, *105*, 473–479. [CrossRef] [PubMed]
69. Grizzle, R.E.; Ward, K.M.; AlShihi, R.M.; Burt, J.A. Current status of coral reefs in the United Arab Emirates: Distribution, extent, and community structure with implications for management. *Mar. Pollut. Bull.* **2016**, *105*, 515–523. [CrossRef] [PubMed]
70. Aboobacker, V.; Samiksha, S.; Veerasingam, S.; Al-Ansari, E.M.; Vethamony, P. Role of shamal and easterly winds on the wave characteristics off Qatar, central Arabian Gulf. *Ocean Eng.* **2021**, *236*, 109457. [CrossRef]
71. Thoppil, P.G.; Hogan, P.J. Persian Gulf response to a wintertime shamal wind event. *Deep. Sea Res. Part I Oceanogr. Res. Pap.* **2010**, *57*, 946–955. [CrossRef]
72. Sandeepan, B.S.; Panchang, V.G.; Nayak, S.; Kumar, K.K.; Kaihatu, J.M. Performance of the WRF Model for Surface Wind Prediction around Qatar. *J. Atmos. Ocean. Technol.* **2018**, *35*, 575–592. [CrossRef]
73. Vieira, F.; Cavalcante, G.; Campos, E. Analysis of wave climate and trends in a semi-enclosed basin (Persian Gulf) using a validated SWAN model. *Ocean Eng.* **2020**, *196*, 106821. [CrossRef]
74. Liao, Y.-P.; Kaihatu, J.M. The effect of wind variability and domain size in the Persian Gulf on predicting nearshore wave energy near Doha, Qatar. *Appl. Ocean Res.* **2016**, *55*, 18–36. [CrossRef]
75. Zhan, C.; Liu, Z.; Zeng, N. Using remote sensing and gis to investigate land use dynamic change in western plain of jilin province. *Int. Arch. Photogramm. Remote Sens. Spat. Inf. Sci.* **2008**, *37*, 1685–1690.
76. Shalaby, A.; Tateishi, R. Remote sensing and GIS for mapping and monitoring land cover and land-use changes in the Northwestern coastal zone of Egypt. *Appl. Geogr.* **2007**, *27*, 28–41. [CrossRef]
77. Mondal, A.; Khare, D.; Kundu, S.; Mondal, S.; Mukherjee, S.; Mukhopadhyay, A. Spatial soil organic carbon (SOC) prediction by regression kriging using remote sensing data. *Egypt. J. Remote Sens. Space Sci.* **2017**, *20*, 61–70. [CrossRef]
78. Huang, C.; Wylie, B.; Yang, L.; Homer, C.; Zylstra, G. Derivation of a tasselled cap transformation based on Landsat 7 at-satellite reflectance. *Int. J. Remote Sens.* **2002**, *23*, 1741–1748. [CrossRef]
79. Baig, M.H.A.; Zhang, L.; Shuai, T.; Tong, Q. Derivation of a tasselled cap transformation based on Landsat 8 at-satellite reflectance. *Remote Sens. Lett.* **2014**, *5*, 423–431. [CrossRef]
80. Zhai, Y.; Roy, D.P.; Martins, V.S.; Zhang, H.K.; Yan, L.; Li, Z. Conterminous United States Landsat-8 top of atmosphere and surface reflectance tasseled cap transformation coefficients. *Remote Sens. Environ.* **2022**, *274*, 112992. [CrossRef]
81. Chen, C.; Fu, J.; Zhang, S.; Zhao, X. Coastline information extraction based on the tasseled cap transformation of Landsat-8 OLI images. *Estuar. Coast. Shelf Sci.* **2019**, *217*, 281–291. [CrossRef]
82. Chen, C.; Chen, H.; Liang, J.; Huang, W.; Xu, W.; Li, B.; Wang, J. Extraction of Water Body Information from Remote Sensing Imagery While Considering Greenness and Wetness Based on Tasseled Cap Transformation. *Remote Sens.* **2022**, *14*, 3001. [CrossRef]
83. Shamsuzzoha, M.; Ahamed, T. Shoreline Change Assessment in the Coastal Region of Bangladesh Delta Using Tasseled Cap Transformation from Satellite Remote Sensing Dataset. *Remote Sens.* **2023**, *15*, 295. [CrossRef]
84. Rivers, J.M.; Dalrymple, R.W.; Yousif, R.; Al-Shaikh, I.; Butler, J.D.; Warren, C.; Skeat, S.L.; Bari, E.M.A. Mixed siliciclastic-carbonate-evaporite sedimentation in an arid eolian landscape: The Khor Al Adaid tide-dominated coastal embayment, Qatar. *Sediment. Geol.* **2020**, *408*, 105730. [CrossRef]
85. Specht, M.; Specht, C.; Lewicka, O.; Makar, A.; Burdziakowski, P.; Dąbrowski, P. Study on the Coastline Evolution in Sopot (2008–2018) Based on Landsat Satellite Imagery. *J. Mar. Sci. Eng.* **2020**, *8*, 464. [CrossRef]
86. Spatio-Temporal Analysis of Texas Shoreline Changes Using GIS Technique. Available online: https://oaktrust.library.tamu.edu/handle/1969.1/408 (accessed on 19 February 2022).
87. Misra, A.; Balaji, R. A Study on the Shoreline Changes and LAND-use/Land-cover along the South Gujarat Coastline. *Procedia Eng.* **2015**, *116*, 381–389. [CrossRef]
88. Mishra, M.; Chand, P.; Pattnaik, N.; Kattel, D.B.; Panda, G.K.; Mohanti, M.; Baruah, U.D.; Chandniha, S.K.; Achary, S.; Mohanty, T. Response of long- to short-term changes of the Puri coastline of Odisha (India) to natural and anthropogenic factors: A remote sensing and statistical assessment. *Environ. Earth Sci.* **2019**, *78*, 338. [CrossRef]

89. Alharbi, O.A.; Phillips, M.R.; Williams, A.T.; Thomas, T.; Hakami, M.; Kerbe, J.; Niang, A.J.; Hermas, E.; Al-Ghamdi, K. Temporal shoreline change and infrastructure influences along the southern Red Sea coast of Saudi Arabia. *Arab. J. Geosci.* **2017**, *10*, 360. [CrossRef]
90. Daoudi, M.; Niang, A.J. Detection of shoreline changes along the coast of Jeddah and its impact on the geomorphological system using GIS techniques and remote sensing data (1951–2018). *Arab. J. Geosci.* **2021**, *14*, 1265. [CrossRef]
91. Niang, A.J. Monitoring long-term shoreline changes along Yanbu, Kingdom of Saudi Arabia using remote sensing and GIS techniques. *J. Taibah Univ. Sci.* **2020**, *14*, 762–776. [CrossRef]
92. Al-Zubieri, A.G.; Ghandour, I.M.; Bantan, R.A.; Basaham, A.S. Shoreline Evolution Between Al Lith and Ras Mahāsin on the Red Sea Coast, Saudi Arabia Using GIS and DSAS Techniques. *J. Indian Soc. Remote Sens.* **2020**, *48*, 1455–1470. [CrossRef]
93. Aldogom, D.; Albesher, S.; Al Mansoori, S.; Nazzal, T. Assessing Coastal Land Dynamics Along UAE Shoreline Using GIS and Remote Sensing Techniques. *IOP Conf. Ser. Earth Environ. Sci.* **2020**, *540*, 012031. [CrossRef]
94. Aladwani, N.S. Shoreline change rate dynamics analysis and prediction of future positions using satellite imagery for the southern coast of Kuwait: A case study. *Oceanologia* **2022**, *64*, 417–432. [CrossRef]
95. Jonah, F.E.; Mensah, E.A.; Edziyie, R.E.; Agbo, N.W.; Adjei-Boateng, D. Coastal Erosion in Ghana: Causes, Policies, and Management. *Coast. Manag.* **2016**, *44*, 116–130. [CrossRef]